REPORT 1105

CHORDWISE AND COMPRESSIBILITY CORRECTIONS TO SLENDER-WING THEORY [1]

By HARVARD LOMAX and LOMA SLUDER

SUMMARY

Corrections to the solutions given by slender-wing theory for the lift distribution on triangular and rectangular wings of low aspect ratio are obtained in two steps. First, slender wing theory is used to find the load distribution over a wing of given shape. Second, the spanwise variation of the loading so obtained is left unchanged but the chordwise variation is modified by satisfying an appropriate integral equation. Results are shown for flat-plate wings and, in the case of the subsonic, triangular wing, a comparison is made with other theoretical solutions and experimental results.

INTRODUCTION

The calculation of loading on three-dimensional lifting surfaces is a fundamental problem in aerodynamic research. The complexity of the problem has led to the development of certain simplified theories by means of which the loading on special types of plan forms can be estimated quickly. The amount of error which these estimates contain is of considerable interest, as are methods which will tend to correct such errors without undue labor.

Slender-wing theory applies to one such simplified body of analysis. There are two basic assumptions of this theory. One, the angle of attack is small enough so that the vortex sheet lies in the plane of the wing and the boundary conditions for the wing can be projected onto a horizontal plane parallel to the direction of the free stream; and the other, that either the chordwise gradient of velocity is small enough or the free-stream Mach number is close enough to unity that the linearized partial differential equation which governs the fluid flow becomes Laplace's equation in a plane transverse to the free-stream direction. References 1 through 6 are examples of papers developing slender-wing theory.

The magnitude of the error of such a theory, in the case of subsonic flow, is indicated by observing solutions for triangular wings. Slender-wing theory gives a finite value for the loading along the trailing edge. Proper inclusion of the chordwise and compressibility effects results in solutions that satisfy the Kutta condition and make the loading fall to zero at the trailing edge. It is the purpose of this report to study such modifications.

The corrections due to the chordwise and compressibility effects are obtained in the following manner: First, an integral equation is set up relating the shape of the wing surface to the lift distribution; second, this integral equation is solved for the given shape under the assumption that the chordwise velocity gradients are small or that the free-stream Mach number is unity; and finally, the integral equation is reinspected for the same wing shape, this time with the spanwise lift distribution fixed at the variation just obtained and with the chordwise variation as the unknown and the Mach number terms included.

Results are presented and discussed both for triangular and rectangular, flat-plate plan forms in both subsonic and supersonic flow.

LIST OF IMPORTANT SYMBOLS

A	aspect ratio $\left(\frac{b^2}{S}\right)$
b	span of wing measured normal to plane of symmetry
c_0	root chord of wing
C_L	lift coefficient $\left(\frac{\text{lift}}{qS}\right)$
C_m	pitching-moment coefficient $\left(\frac{\text{pitching moment about leading edge or apex}}{qSc_0}\right)$
$E(t,k)$	incomplete elliptic integral of the second kind with argument t and modulus k $\left[E(t,k)=\int_0^t\sqrt{\frac{1-k^2t^2}{1-t^2}}\,dt\right]$
E	complete elliptic integral of second kind, $E(1,k)$
$F(t,k)$	incomplete elliptic integral of the first kind with argument t and modulus k $\left[F(t,k)=\int_0^t\frac{dt}{\sqrt{(1-t^2)(1-k^2t^2)}}\right]$
K	complete elliptic integral of first kind, $F(1,k)$
m	for triangular wing, slope of leading edge relative to plane of symmetry
M_0	free-stream Mach number $\left(\frac{V_0}{\text{speed of sound in free stream}}\right)$
p	static pressure
Δp	p_l-p_u
q	free-stream dynamic pressure $\left(\frac{1}{2}\rho_0 V_0^2\right)$
s	semispan of rectangular wing
S	area of wing

[1] Supersedes NACA TN 2295, "Chordwise and Compressibility Corrections to Slender-Wing Theory," by Harvard Lomax and Loma Sluder, 1951.

272483—54——67

u	perturbation velocity component in the direction of the x axis
Δu	u_u-u_l
V_0	free-stream velocity
w	perturbation velocity component in the direction of the z axis
w_0	$-V_0\alpha$
x,y,z	Cartesian coordinates of an arbitrary point
x_1,y_1	Cartesian coordinates of source or doublet position
x_0	$\frac{x}{c_0}$
α	angle of attack
β	$\sqrt{\lvert 1-M_0^2\rvert}$
θ_0	βm
ρ_0	density in free stream
σ, σ_p	doublet weighting factors
φ	perturbation velocity potential
$\Delta\varphi$	$\varphi_u-\varphi_l$

SUBSCRIPTS

l	conditions on lower surface of wing (at $z=0-$)
u	conditions on upper surface of wing (at $z=0+$)

THE INTEGRAL EQUATIONS

SUBSONIC

Triangular plan form.—A general solution of Laplace's equation which is suited to problems in linearized subsonic wing theory (given, e. g., in reference 7) is that which relates a velocity potential or perturbation velocity to the value of its jump across a given surface. For the lifting triangular wing shown in figure 1 this can be written

$$u=\frac{z\beta^2}{4\pi}\int_0^{c_0}dx_1\int_{-mx_1}^{mx_1}\frac{\Delta u\,dy_1}{[(x-x_1)^2+\beta^2(y-y_1)^2+\beta^2z^2]^{3/2}} \quad (1)$$

where $\beta=\sqrt{\lvert 1-M_0^2\rvert}$, u is the perturbation velocity parallel to the x axis, and Δu is the jump in u over the wing plan form.

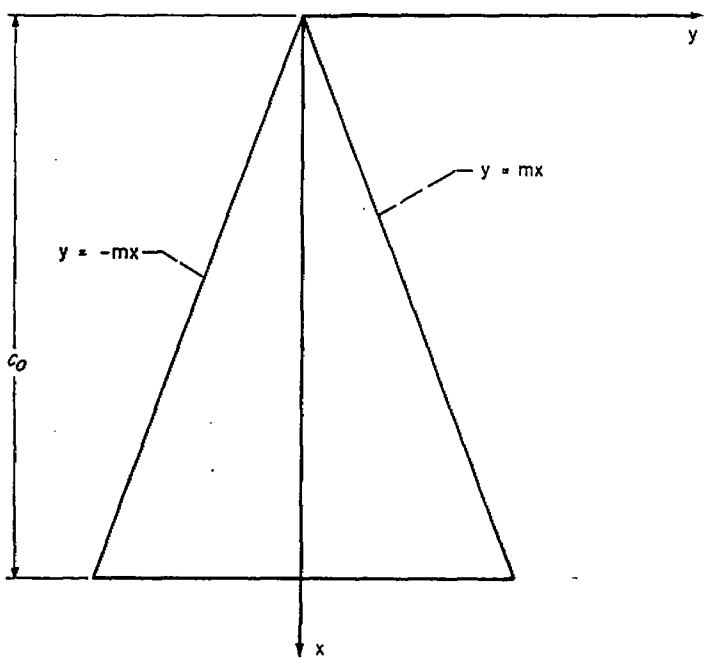

FIGURE 1.—Triangular-wing coordinate system.

In linearized theory this jump can be related to the loading coefficient $\Delta p/q$ by the equation

$$\Delta u=\frac{V_0}{2}\left(\frac{\Delta p}{q}\right) \quad (2)$$

Further, the velocity potential φ can be found by the relation

$$\varphi=\int_{-\infty}^{x}u\,dx$$

Operating on equation (1) in this manner and interchanging the order of integration gives

$$\varphi=\frac{z\,V_0}{8\pi}\int_0^{c_0}dx_1\int_{-mx_1}^{mx_1}\frac{\left(\frac{\Delta p}{q}\right)dy_1}{[(y-y_1)^2+z^2]}\left[1+\frac{x-x_1}{\sqrt{(x-x_1)^2+\beta^2z^2+\beta^2(y-y_1)^2}}\right] \quad (3)$$

which represents, physically, a distribution of elementary horseshoe vortices.

The effect of compressibility in a linearized study of lifting-surface theory can only enter through the use of β. Setting

$$\sigma=1+\frac{x-x_1}{\sqrt{(x-x_1)^2+\beta^2(y-y_1)^2+\beta^2z^2}} \quad (4)$$

it is seen that σ is the only term in equation (3) which contains β. This term has an interesting interpretation in the light of the study which has been made at sonic speeds. At $M_0=1$ (i. e., $\beta=0$), σ has either the value 2 or 0, depending on whether x_1 is less or greater than x. Hence, for $M_0=1$, equation (3) becomes

$$\varphi=\frac{z\,V_0}{4\pi}\int_0^{x}dx_1\int_{-mx_1}^{mx_1}\frac{\left(\frac{\Delta p}{q}\right)dy_1}{(y-y_1)^2+z^2} \quad (5)$$

Now reversing the order of integration and using the definition implied by equation (2), namely,

$$\frac{\Delta p}{q}=\frac{2}{V_0}\frac{\partial\Delta\varphi}{\partial x_1}$$

gives finally

$$\varphi=\frac{z}{2\pi}\int_{-mx}^{mx}\frac{\Delta\varphi\,dy_1}{(y-y_1)^2+z^2} \quad (6)$$

Equation (6) has been studied in reference 5 as the fundamental equation for slender wings or wings flying at near sonic speeds. It is an equation which gives the solution for the velocity potential in a three-dimensional flow in terms of two-dimensional doublets, the two dimensions being at right angles to the free-stream direction. A solution of such a nature is immediately implied by the physical character of both sonic wing theory, in which the Mach cone has degenerated to a Mach plane, and slender-wing theory, in which the wing is so slender that the chordwise gradient of velocities can be neglected compared to the vertical and lateral gradients.

By comparison of equation (5) with equation (3), it is seen that the term σ can be interpreted as a factor which corrects the slender-wing-theory results as given by equation (5) for the effects of chordwise gradients in velocity and

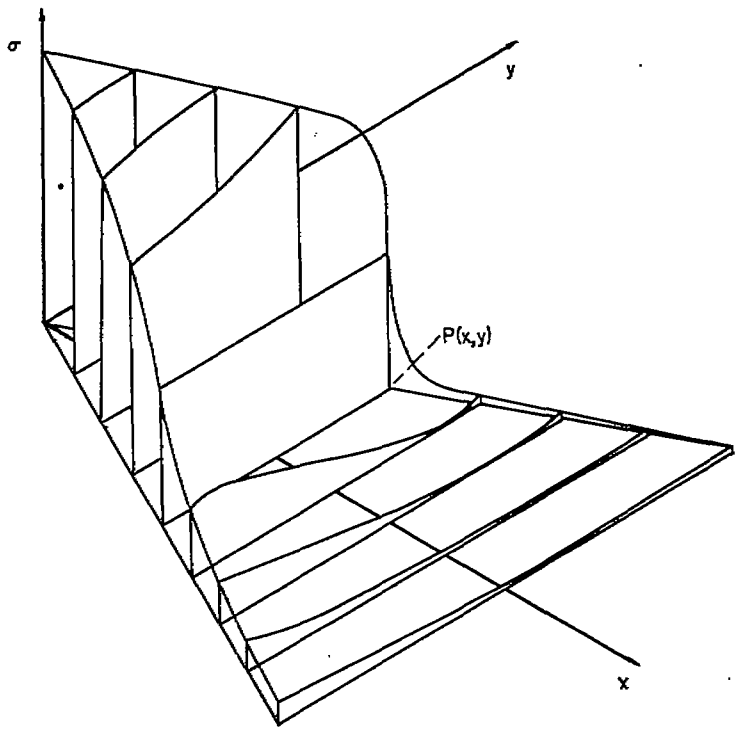

FIGURE 2.—Typical variation of σ over a triangular wing.

compressibility. By consideration of the effect at one point of the distribution of doublets over the wing, this correction can be visualized as a reweighting of the two-dimensional doublets according to their position relative to the point. Figure 2 indicates the variation of σ across the span at various chord stations for $\beta=0.6$. Observe that the doublets ahead of the point at which the potential is to be determined are still weighted far more heavily than those behind the point. The effect of considering β different from zero, however, is to reduce the extreme difference in weight occasioned at $\beta=0$ so that the doublets behind a given point do have some effect on the induced velocities there, and the doublets ahead of a point induce a somewhat smaller disturbance than before. Since the strength of these weighted two-dimensional doublets is given by the magnitude of the three-dimensional loading, their strength is zero everywhere off the wing plan form including the area behind the wing occupied by the vortex wake.

Two different methods for the further reduction of equation (3) will be considered. The first method involves finding the vertical induced velocity for points along the x axis, while the second involves finding the average vertical induced velocity along the span at a given chord station. The first method must be discarded for triangular wings because of difficulties around the apex; the second, however, proves to be satisfactory. The simplification obtained by considering the vertical induced velocity for points along the x axis will be considered later in connection with the rectangular wing.

Since it is easier to consider first the averaging process, the operator

$$\lim_{z\to 0}\frac{1}{2mx}\frac{\partial}{\partial z}\int_{-mx}^{mx}dy$$

is applied to the weighted doublets, $\sigma z/[(y-y_1)^2+z^2]$, of equation (3) with the result that

$$\overline{w}=-\frac{V_0}{8\pi}\int_0^{c_0}dx_1\int_{-mx_1}^{mx_1}dy_1\frac{\left(\frac{\Delta p}{q}\right)}{m^2x^2-y_1^2}-\frac{V_0}{8\pi}\int_0^{c_0}dx_1\int_{-mx_1}^{mx_1}\frac{\left(\frac{\Delta p}{q}\right)dy_1}{2mx(x-x_1)}$$
$$\left[\frac{\sqrt{(x-x_1)^2+\beta^2(mx-y_1)^2}}{mx-y_1}+\frac{\sqrt{(x-x_1)^2+\beta^2(mx+y_1)^2}}{mx+y_1}\right] \quad (7)$$

where $\overline{w}$ is the average value of the vertical induced velocity along a given span.

The solution for $\Delta p/q$ obtained from slender-wing theory can be written [2]

$$\frac{\Delta p}{q}=-\frac{4w_0m^2x_1}{V_0\sqrt{m^2x_1^2-y_1^2}}f_1\left(\frac{x_1}{c_0}\right) \quad (8)$$

where in that theory $f_1(x_1/c_0)=1$. If the value of $\Delta p/q$ given by equation (8) is placed in equation (7), the resulting integral equation can be written in a simplified form if it is noted that

$$I_1=\int_{-mx_1}^{mx_1}\left[\frac{\sqrt{(x-x_1)^2+\beta^2(mx-y_1)^2}}{mx-y_1}+\frac{\sqrt{(x-x_1)^2+\beta^2(mx+y_1)^2}}{mx+y_1}\right]\frac{\frac{1}{2}m\,dy_1}{\sqrt{m^2x_1^2-y_1^2}}$$
$$=m\int_{m(x-x_1)}^{m(x+x_1)}\frac{\sqrt{(x-x_1)^2+\beta^2\eta^2}\,d\eta}{\eta\sqrt{-m^2(x^2-x_1^2)+2\eta mx-\eta^2}} \quad (9)$$

where for the first term in the brackets the transformation $\eta=mx-y_1$ was used and for the second the transformation $\eta=mx+y_1$. Hence, equation (7) finally reduces to the following

$$\overline{w}=\frac{w_0}{2\pi x}\left[\int_0^x\frac{\pi x_1f_1\left(\frac{x_1}{c_0}\right)}{\sqrt{x^2-x_1^2}}\,dx_1+\int_0^{c_0}\frac{x_1I_1f_1\left(\frac{x_1}{c_0}\right)}{(x-x_1)}\,dx_1\right] \quad (10)$$

The solution of equation (10) will be discussed in a later section devoted to triangular wings.

Rectangular plan form.—If the plan form of the wing is rectangular as shown in figure 3, then equation (3) is modified slightly to the form

$$\varphi=\frac{zV_0}{8\pi}\int_0^{c_0}dx_1\int_{-s}^{s}\frac{\sigma\frac{\Delta p}{q}\,dy_1}{(y-y_1)^2+z^2} \quad (11)$$

It is possible in this case to study the vertical induced velocity for points along the x axis; that is, to find $\partial\varphi/\partial z$ by equation (11) and then set both y and z equal to zero. In order to do this a special notation is employed. Thus, if the indefinite integral of $f(y)/y^2$ can be written (where $f(y)$ is bounded at $y=0$)

$$\int\frac{f(y)}{y^2}\,dy=J(y)+C$$

then, by definition,

$$\oint_{-s}^{s}\frac{f(y)}{y^2}\,dy\equiv J(s)-J(-s) \quad (12)$$

By means of this definition it can be shown (see reference 8) that

[2] This solution follows from an analysis of equation (6). See reference 5.

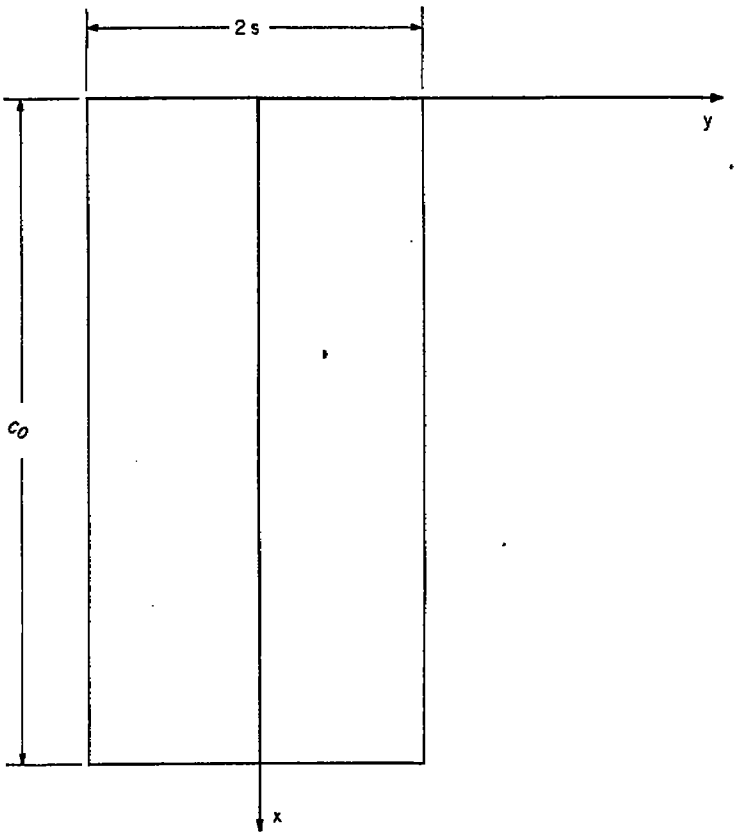

FIGURE 3.—Rectangular-wing coordinate system.

$$w=\frac{V_0}{8\pi}\int_0^{c_0}dx_1\fint_{-s}^{s}dy_1\left(\frac{\Delta p}{q}\right)\frac{1}{y_1^2}\left[1+\frac{x-x_1}{\sqrt{(x-x_1)^2+\beta^2y_1^2}}\right] \quad (13)$$

If [3]

$$\frac{\Delta p}{q}=-4\,\frac{w_0}{V_0c_0}\,f_2\left(\frac{x}{c_0}\right)\sqrt{s^2-y^2} \quad (14)$$

integration by parts gives

$$I_2=-(x-x_1)^2\fint_{-s}^{s}\frac{dy_1}{y_1^2}\sqrt{\frac{s^2-y_1^2}{(x-x_1)^2+\beta^2y_1^2}}$$

$$=\int_{-s}^{s}\sqrt{\frac{(x-x_1)^2+\beta^2y_1^2}{s^2-y_1^2}}\,dy_1 \quad (15)$$

and equation (13) can be written

$$w=\frac{w_0}{2\pi c_0}\int_0^{c_0}\left(\pi+\frac{I_2}{x-x_1}\right)f_2\left(\frac{x_1}{c_0}\right)dx_1 \quad (16)$$

This integral equation has been derived previously by K. Wieghardt (reference 9) with regard to the rectangular-wing problem. The solution of equation (16) will be discussed in a later section devoted to rectangular wings.

SUPERSONIC

Triangular plan form.—In passing from subsonic to supersonic theory, we pass from the elliptic to the hyperbolic partial differential equation and in particular from Laplace's equation to the wave equation. The solution which relates the perturbation velocity u at any point in the field to the loading on the wing can again be written in terms of an elementary horseshoe vortex distribution over the wing plan form. As in reference 8, this becomes

$$u=\frac{z}{2\pi}\frac{\partial}{\partial x}\iint_\tau\frac{(x-x_1)\Delta u\,dx_1dy_1}{[(y-y_1)^2+z^2]\sqrt{(x-x_1)^2-\beta^2(y-y_1)^2-\beta^2z^2}}$$

and since $u=\frac{\partial\varphi}{\partial x}$ and $\frac{\Delta p}{q}=\frac{2\Delta u}{V_0}$,

$$\varphi=\frac{V_0z}{4\pi}\iint_\tau\frac{\frac{\Delta p}{q}\,dx_1dy_1}{(y-y_1)^2+z^2}\left[\frac{x-x_1}{\sqrt{(x-x_1)^2-\beta^2(y-y_1)^2-\beta^2z^2}}\right] \quad (17)$$

where τ is the area on the wing bounded by the edges and the trace of the Mach forecone from the point x, y, z. Again the effect of compressibility appears only in the term within the brackets. Hence, setting

$$\sigma_p=\frac{x-x_1}{\sqrt{(x-x_1)^2-\beta^2(y-y_1)^2-\beta^2z^2}} \quad (18)$$

σ_p contains all of the Mach number effects at supersonic speeds. At $M_0=1$, $\sigma_p=1$, and since, by the definition of τ, $x_1\leq x$, it follows that at sonic speeds equation (17) also reduces to equation (5). Therefore the doublet distributions represented by equations (17) and (3) are consistent at the speed of sound.

In order that an exact parallel can be provided with the subsonic solution to the triangular wing, the average vertical induced velocity for points along a given span is again considered. It can be shown (reference 8) that in the plane of the wing

$$w=-\frac{\beta V_0}{4}\frac{\Delta p}{q}+\frac{V_0}{4\pi}R.P.\int_0^x dx_1\fint_{-mx_1}^{mx_1}dy_1$$

$$\frac{(x-x_1)\frac{\Delta p}{q}}{(y-y_1)^2\sqrt{(x-x_1)^2-\beta^2(y-y_1)^2}} \quad (19)$$

where the order of integration must be carried out as indicated (i. e., the integration with respect to y_1 must be made first). The letters *R. P.* mean that the real part of the term is to be taken. Such a device can be used since the double integral must always be a pure real quantity in the area τ ($\Delta p/q$ is real everywhere on the plan form) and a pure imaginary quantity over the rest of the area indicated by the limits on the integrals (see fig. 4). The average vertical induced velocity along the span may be obtained by applying to equation (19) the operator

$$\frac{1}{2mx}\int_{-mx}^{mx}dy$$

and since

$$\frac{\Delta p}{q}=-\frac{4w_0m^2x_1}{V_0\sqrt{m^2x_1^2-y_1^2}}\,f_3(x_1) \quad (20)$$

equation (19) may be written in the form

$$\overline{w}=\frac{\pi\beta mw_0f_3(x)}{2}+\frac{w_0}{\pi x}\int_0^x\frac{x_1I_3f_3(x_1)dx_1}{x-x_1} \quad (21)$$

[3] The solution for the rectangular wing given by slender-wing theory is that the load be zero across every spanwise strip aft of the leading edge. To find the chordwise correction to such a theory, therefore, a spanwise distribution must be assumed. Since, however, slender-wing theory also requires an elliptical span loading for the boundary conditions of a rectangular wing to be satisfied, a reasonable choice is that given by equation (14).

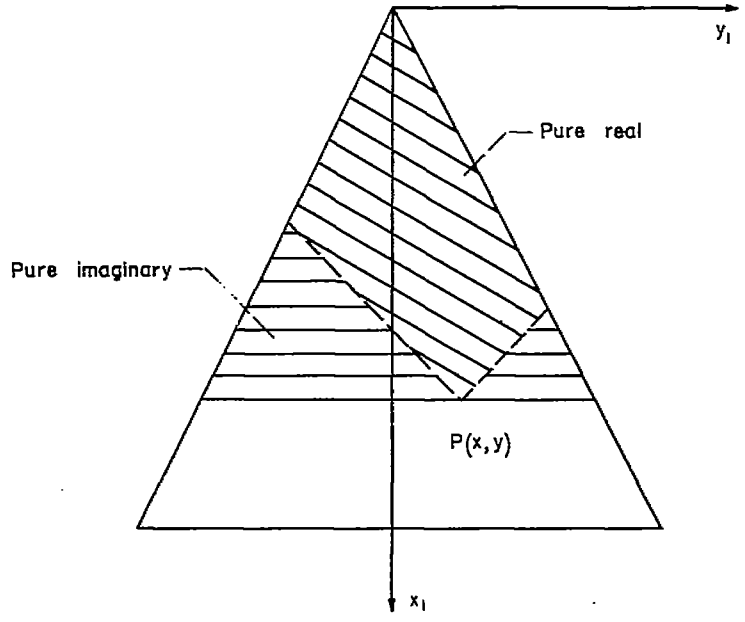

FIGURE 4.—Regions for which the double integral term in equation (19) is a pure real or pure imaginary.

The derivation of I_3 is similar to that used for equation (9) and leads to the expression

$$I_3 = m\,R.P.\int_{m(x-x_1)}^{m(x+x_1)} \frac{\sqrt{(x-x_1)^2-\beta^2\eta^2}\,d\eta}{\eta\sqrt{[m(x_1+x)-\eta]\,[m(x_1-x)+\eta]}} \tag{22}$$

It is possible to find an exact solution for $f_3(x)$ by means of equation (21), but the discussion of this analysis is reserved for a subsequent section.

Rectangular plan form.—Equation (19) can also be used in the case of a rectangular plan form by an appropriate change in limits; thus,

$$w = -\frac{\beta V_0 \frac{\Delta p}{q}}{4} + \frac{V_0}{4\pi} R.P.\int_0^x dx_1 \overline{\int_{-s}^{s}} dy_1 \frac{(x-x_1)\frac{\Delta p}{q}}{(y-y_1)^2\sqrt{(x-x_1)^2-\beta^2(y-y_1)^2}} \tag{23}$$

where again it should be stressed that the order of integration cannot be reversed. The regions in which the integration yields real or imaginary results are shown in figure 5. As in the case of the subsonic rectangular wing, the value of w will be obtained only along the x axis so that y in equation (23) can be set equal to zero. The loading will be assumed to have a form

$$\frac{\Delta p}{q} = -4\frac{w_0}{V_0 s\beta} f_4\left(\frac{x}{s\beta}\right)\sqrt{s^2-y^2} \tag{24}$$

which is similar to that used in the subsonic case except that the reference length is now the semispan instead of the chord. Such a difference is reasonable since in the supersonic case the position of the trailing edge cannot affect the loading on the wing.

Finally, therefore, when $y=0$ equation (23) becomes

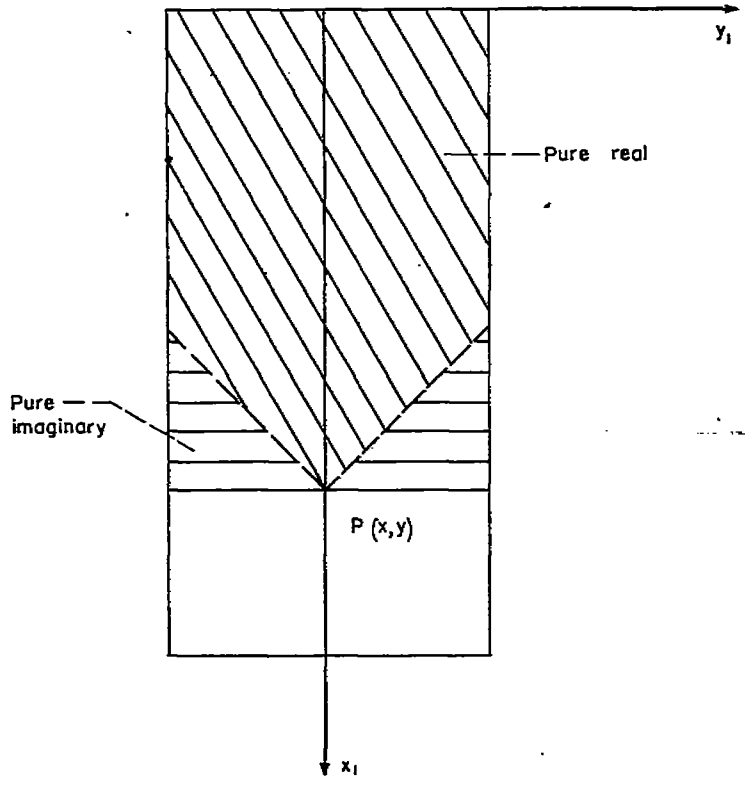

FIGURE 5.—Regions for which the double integral term in equation (23) is pure real or pure imaginary.

$$w = w_0 f_4\left(\frac{x}{s\beta}\right) + \frac{w_0}{\pi s\beta}\int_0^x \frac{I_4 f_4\left(\frac{x_1}{s\beta}\right)}{x-x_1} dx_1 \tag{25}$$

where I_4 is given by the equation

$$I_4 = R.P.\int_{-s}^{s}\sqrt{\frac{(x-x_1)^2-\beta^2 y_1^2}{s^2-y_1^2}}\,dy_1 \tag{26}$$

The solution of equation (25) is deferred to a subsequent section.

LOADING ON WINGS

The previous section was devoted to the development of the integral equations which are to be studied for the two types of plan forms in subsonic and supersonic flight. In order that this study can proceed in a natural manner, the arrangement of the presentation has been changed so that the plan form is the principal division and the speed is subsidiary.

TRIANGULAR WINGS

Supersonic case.—The decision to solve for the loading on the supersonic, triangular, flat plate by analyzing equation (21) was not an obvious one since the exact solution of the linearized partial differential equation for this case has already been obtained. (See, e. g., references 10, 11, and 12.) Thus it is known before starting that the value of $f_3(x)$ in equation (21) must be $1/E$ where E is the complete elliptic integral of the second kind with modulus $\sqrt{1-m^2\beta^2}$. However, these solutions were obtained by an entirely different procedure so that by solving equation (21) and comparing the two results a check on the accuracy of the method is obtained. Furthermore, when the subsonic

problem is analyzed the same general procedure will be followed and the results can then be accepted with greater confidence.

The first step in the solution of equation (21), in which $\overline{w}$ has been set equal to w_0 since the wing is a flat plate, is to change variables by the transformation $\xi_1=x_1/x$. This gives

$$1=\frac{\pi\beta m}{2}f_3(x)+\frac{1}{\pi}\int^1\frac{\xi_1 f_3(x\xi_1)d\xi_1}{1-\xi_1}I_3(\xi_1) \tag{27}$$

In the equation for I_3, the transformation $m\eta_1=\eta/x$ was used so that

$$I_3=\int_{1-\xi_1}^{1+\xi_1}\frac{\sqrt{(1-\xi_1)^2-\beta^2m^2\eta_1^2}}{\eta_1\sqrt{(\xi_1+1-\eta_1)(\xi_1-1+\eta_1)}}d\eta_1$$

which is completely independent of x. The partial derivative of both sides of equation (27) with respect to x gives

$$f_3'(x)=-\frac{2}{\pi^2\beta m}\int_0^1\frac{\xi_1^2 f_3'(x\xi_1)d\xi_1}{1-\xi_1}I_3(\xi_1) \tag{28}$$

Equation (28) is a homogeneous linear integral equation. The solution to equation (28) is simply $f_3'(x)=0$ or, what is equivalent, $f_3(x)$ equals a constant, $(f_3)_0$ say. By means of equation (27), this constant can be evaluated. Hence,

$$(f_3)_0=\left[\frac{\pi\beta m}{2}+\frac{1}{\pi}\int_0^1\frac{\xi_1 I_3(\xi_1)d\xi_1}{1-\xi_1}\right]^{-1} \tag{29}$$

which represents the solution to the problem. The integral I_3 was calculated analytically as in appendix A, and then the value of $(f_3)_0$, as given by equation (29), was determined by numerical integration. For $\beta m=0.8$ the result of this computation was 0.708; whereas the true value given by $1/E$ is 0.705.

Equation (27) can also be solved when the wing is slender with respect to the Mach cone by considering βm to be small. Setting $\beta m=0$ yields

$$(I_3)_{\beta m=0}=(1-\xi_1)\int_{(1-\xi_1)}^{(1+\xi_1)}\frac{d\eta_1}{\eta_1\sqrt{(\xi_1+1-\eta_1)(\xi_1-1+\eta_1)}}$$

and this is readily evaluated to give

$$(I_3)_{\beta m=0}=\frac{\pi(1-\xi_1)}{\sqrt{1-\xi_1^2}} \tag{30}$$

The integral equation reduces to

$$1=\int_0^1\frac{\xi_1 f_3(x\xi_1)d\xi_1}{\sqrt{1-\xi_1^2}}$$

which by a retransformation of variables $x_1=x\xi_1$ becomes

$$x=\int_0^x\frac{x_1 f_3(x_1)dx_1}{\sqrt{x^2-x_1^2}} \tag{31}$$

Equation (31) is a special form of Abel's integral equation, the unique inversion [4] of which is, in this case, $f_3(x)=1$. This is easily verified by direct substitution.

The simplicity of this result is not accidental, of course, since the value of $f_3(x)$ was originally introduced by equation (20) as a correction factor to the slender-wing-theory solution.

Subsonic case.—The study of the triangular wing presented in the preceding section was made first at arbitrary supersonic Mach numbers and then at a Mach number equal to 1. In keeping with this order of decreasing speed, the subsonic flat plate will be studied first at sonic speed and then for general subsonic Mach numbers.

An inspection of equations (9) and (22) is sufficient to show that $(I_1)_{\beta m=0}$ is equal to $(I_3)_{\beta m=0}$. Hence, equation (30) can be substituted into equation (10) and there results (since again $\overline{w}$ is set equal to w_0)

$$1=\frac{1}{2\pi x}\left[\int^x\frac{\pi x_1 f_1\left(\frac{x_1}{c_0}\right)dx_1}{\sqrt{x^2-x_1^2}}+\int_0^x\frac{\pi x_1 f_1\left(\frac{x_1}{c_0}\right)dx_1}{\sqrt{x^2-x_1^2}}\right]$$

and this reduces immediately to

$$x=\int_0^x\frac{x_1 f_1\left(\frac{x_1}{c_0}\right)dx_1}{\sqrt{x^2-x_1^2}} \tag{32}$$

It is now obvious that equation (31), which was derived from supersonic wing theory, and equation (32), which was derived from subsonic wing theory, are identical. Clearly this establishes the continuity of the theory in passing from the supersonic to the subsonic regimes.

The study of the general subsonic case leads eventually to the numerical solution of an integral equation. However, an idea of the qualitative form which this solution must assume can be gained by some preliminary analysis.

First write equation (10) in the form

$$1=\frac{1}{2\pi x_0}\left[\int^{x_0}\frac{\pi x_2 f_1(x_2)dx_2}{\sqrt{x_0^2-x_2^2}}+\int_0^1\frac{x_2 I_1\left(\frac{x_2}{x_0}\right)f_1(x_2)dx_2}{x_0-x_2}\right] \tag{33}$$

where $x_0=x/c_0$, $x_2=x_1/c_0$, and $\overline{w}/w_0=1$. The evaluation of I_1 is given in appendix A, and a plot of $\frac{1}{2}I_1$ against x_2/x_0 for $(\beta m)^2$ equal to 0, 0.05, 0.10, and 0.20 is shown in figure 6. Obviously equation (33) is a singular integral equation. We have already seen that for $\beta m=0$ it is an Abel type integral equation with a ½-power singularity at the upper

[4] If Abel's equation is written in the form

$$f(y)=\int_a^y\frac{g(x)dx}{\sqrt{y-x}}$$

its inversion is

$$g(x)=\frac{1}{\pi}\frac{d}{dx}\int_a^x\frac{f(y)dy}{\sqrt{x-y}}$$

and this inversion is unique for functions $g(x)$ that fulfill the condition

$$\lim_{\epsilon\to 0}\ g_\epsilon(x\pm\epsilon)=0\ ,\ a\leq x\leq y \tag{a}$$

Since the solutions for the velocity throughout the flow field must also satisfy condition (a), the value of $g(x)$ given above is unique in the class of functions available.

limit. For finite values of βm, however, I_1 is seen from figure 6 to be bounded and nonzero in the interval $0 \leq x_2/x_0 < \infty$; hence, for such βm, equation (33) is a combination of two types of singular integral equations, the Abel type and the Cauchy type, the latter having a first-power singularity in the interval of integration.

Experience with the Cauchy type integral equation

$$f(y)=\int_0^1 \frac{g(x)dx}{y-x} \tag{34}$$

which arises, for example, in the study of subsonic lifting-line theory and two-dimensional airfoil theory is useful in the present problem. Thus, the solution to equation (34) is not unique (even when $g(x)$ is restricted according to equation (a) in footnote 4) unless some additional condition is given. Such a condition might be the requirement that $g(1)=0$; this would correspond in two-dimensional airfoil theory to the specification of the Kutta condition at the trailing edge. Further, it is known that if the condition $g(1)=0$ is satisfied in equation (34), then $g(x)$ tends to infinity as x approaches zero.

Since the solution to equation (33) must also satisfy the Kutta condition, the above discussion leads one to anticipate for the shape of $f_1(x_0)$ a curve something like that shown in figure 7 (a). On the basis of such qualitative knowledge, a simple numerical procedure was set up and used to calculate the solution to equation (33). This procedure, which is based on the assumption that $f_1(x_0)$ is constant over each of nine equally spaced intervals, is presented in appendix B. The results of the analysis for $(\beta m)^2$ equal to 0.1 (i. e., $\beta A=1.26$) are shown in figure 7 (b).

In order to check the results derived from the method just mentioned, equation (33) has been solved in an alternative manner. In this second approach it is assumed that $f_1(x_0)$ can be approximated by a second degree polynomial which is multiplied by two factors, one that vanishes for $x_0=1$ and the other that tends to infinity as x_0 vanishes.

First consider the behavior of $f_1(x_0)$ for small x_0. A brief study of the solutions to the two integral equations represented by equations (32) and (34) will illustrate how $f_1(x_0)$ can be analyzed in the vicinity of the origin. First consider the Cauchy type integral equation (34) and assume that for x small $g(x)$ can be expressed in the form

$$g(x)=\frac{1}{x^\delta}\sum_{n=0}^{\infty} a_n x^n, \qquad 1>\delta>0$$

Then equation (34) becomes

$$f(y)=a_0\int_0^1 \frac{dx}{x^\delta(y-x)}-\sum_{n=1}^{\infty} a_n \int_0^1 \frac{x^{n-\delta}dx}{x-y}$$

which in the limit as $y\to 0$ reduces to

$$f(0)+\sum_{n=1}^{\infty}\frac{a_n}{n-\delta}=\lim_{y\to 0} a_0\int_0^1 \frac{dx}{x^\delta(y-x)}$$

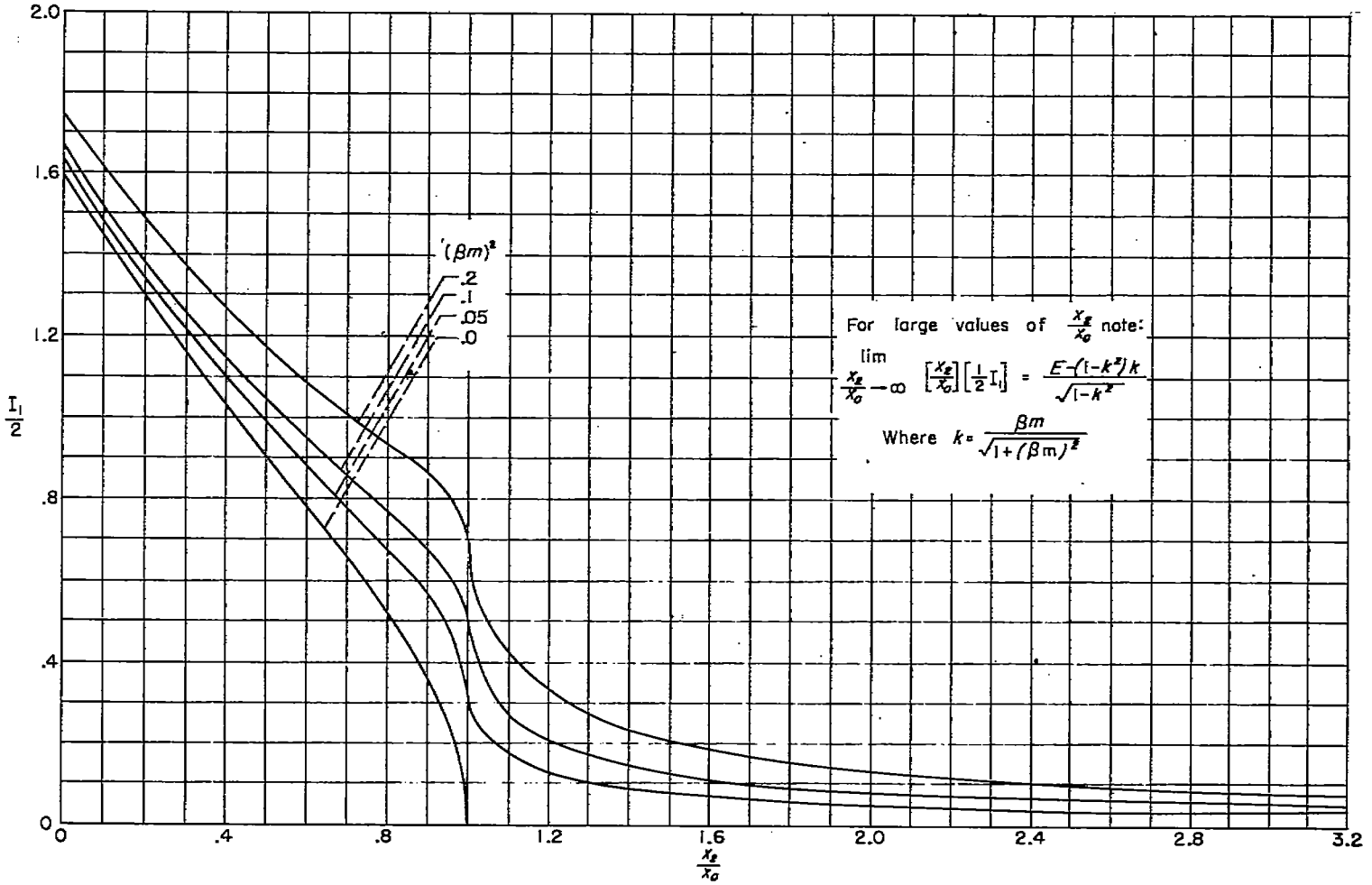

FIGURE 6.—Variation of $I_1/2$ with x_2/x_0.

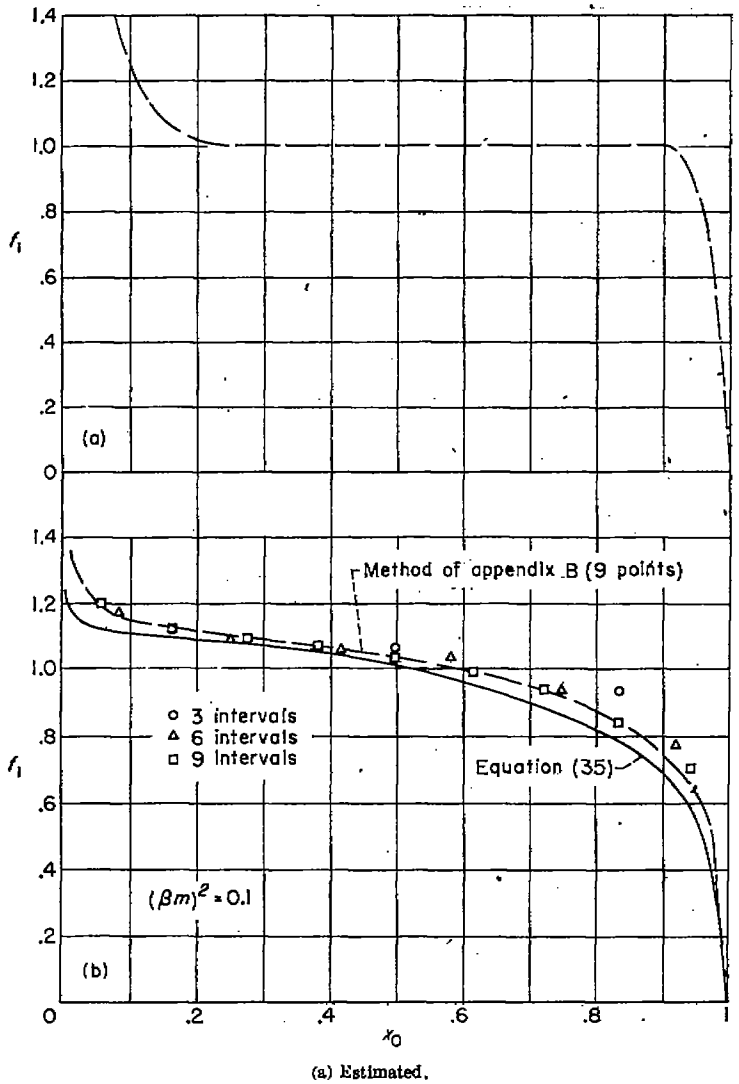

(a) Estimated.
(b) Calculated.

FIGURE 7.—Variation of f_1 with x_0.

or, setting $x=y\xi$, to

$$\lim_{y\to 0} \frac{1}{y^\delta}\int_0^{1/y} \frac{d\xi}{\xi^\delta(1-\xi)} = \frac{1}{a_0}\left[f(0)+\sum_{n=1}^{\infty}\frac{a_n}{n-\delta}\right]$$

The term on the left is indeterminate and implies

$$\lim_{y\to 0}\int_0^{1/y} \frac{d\xi}{\xi^\delta(1-\xi)} = \int_0^{\infty} \frac{d\xi}{\xi^\delta(1-\xi)} = \pi \cot[(1-\delta)\pi] = 0$$

This equality is satisfied, since δ is to be greater than zero and less than 1, only by the value $\delta=\frac{1}{2}$. The fact that this must be the exponent of $1/x$ in the expression for $g(x)$ can be verified by inspecting the known solution to equation (34).

A similar analysis applied to Abel's integral equation in the form given by equation (32) shows for that case δ must be zero which, again, agrees with the known inversion.

Finally, in appendix C this same approach is used to discover the initial behavior of $f_1(x_0)$ in equation (33). Figure 8 presents the results of this analysis throughout the range of βA for which I_1 was calculated.

As was already mentioned, the variation of $f_1(x_0)$ in the vicinity of $x_0=1$, that is, near the trailing edge of the wing, is fixed by the Kutta condition. A useful statement of this condition that holds in both subsonic and supersonic flow is

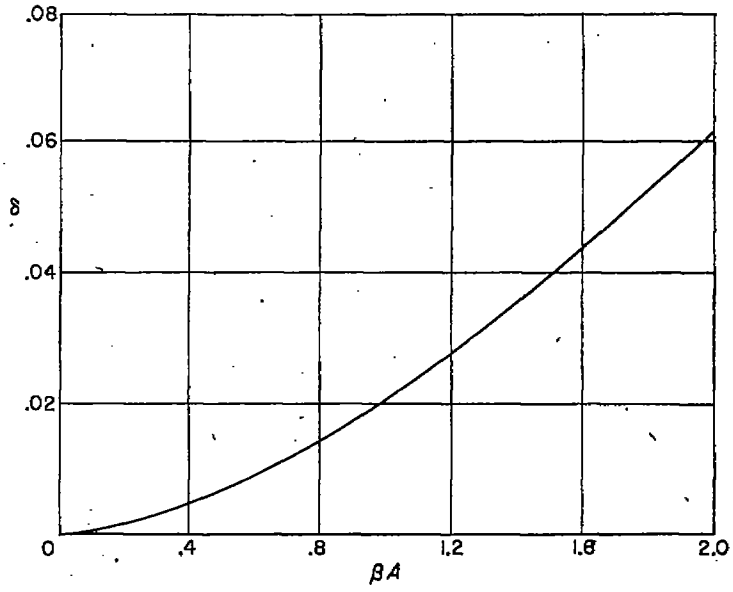

FIGURE 8.—Variation of δ with reduced aspect ratio βA.

that the magnitude of the loading at the trailing edge must not be infinite. However, the only pertinent solution to equation (34), and hence to equation (33), that is not infinite at $x=1$ is that which is identically zero there. Further, as the trailing edge of the triangular wing is more and more closely approached, it is reasonable to expect that the shape of the load distribution in its vicinity approaches that in the vicinity of a simple two-dimensional wing trailing edge, the effect of the wing plan form vanishing as the ratio of the distance from the leading to trailing edge tends to infinity. On the basis of these considerations, $f_1(x_0)$ should approach zero as the term $(1-x_0)^{\frac{1}{2}}$ approaches zero when x_0 tends to 1.

It is also apparent, however, that $f_1(x_0)$ equals 1 for all x_0 between zero and 1 when the Mach number is unity. Further, as M_0 approaches 1 or as the angle of sweep approaches 90°, the effect of the plan form on the shape of the loading near the trailing edge becomes increasingly important or, in other words, the trailing edge of the triangular wing must be more and more closely approached before the shape of the two-dimensional load distribution is simulated. An exponent to $(1-x_0)$ which satisfies this requirement as well as those in the preceding paragraph is $\gamma/2(\gamma+1-x_0)$ where γ is a function of Mach number and vanishes as $M_0\to 1$.

Finally, therefore, it is assumed that $f_1(x_0)$ can be expressed by the equation

$$f_1(x_0) = \frac{(1-x_0)^{\gamma/2(\gamma+1-x_0)}}{x_0^{\delta}}(a_0+a_1x_0+a_2x_0^2) \qquad (35)$$

The values of the constants a_0, a_1, a_2, and γ are determined by satisfying equation (33) at four chordwise stations and are given for $(\beta m)^2$ equal to 0, 0.1, and 0.2 in table I. The accuracy to which these solutions satisfy the integral equation is indicated by table II.

A comparison, for $(\beta m)^2=0.1$, between the solution given by equation (35) and that derived by the method outlined in appendix B is shown in figure 7 (b). The strictly numerical method presented in the appendix was used for three different interval spacings, results for which are indicated in the figure by the symbols. Presumably the accuracy of the method

increases with increasing number of intervals used. A study of the figure shows that the numerical method is apparently approaching [5] the solution given by equation (35). Subsequent values in this report are based on the solutions represented by the latter equation.

The final curves for $f_1(x_0)$ are shown in figure 9. A discussion of the integrated values of the loading will be given later.

RECTANGULAR WINGS

The discussion of the triangular wing was divided according to the Mach number. The same division will be used in this section, starting with the discussion of the results for supersonic speeds, then with that for both supersonic and subsonic theories at sonic speeds, and closing with a discussion of the subsonic development.

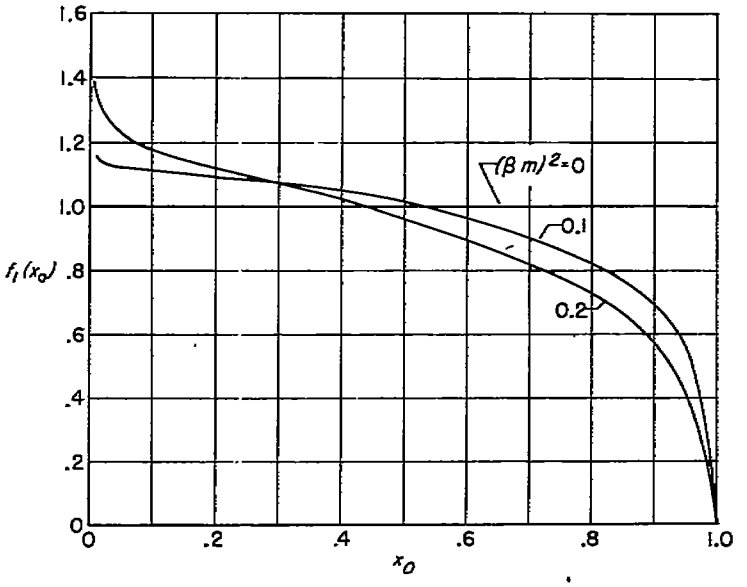

FIGURE 9.—Final values of $f_1(x_0)$ given by equation (35) and table I.

Supersonic case.—The solution of equation (25) will give the loading on a rectangular wing flying at a supersonic Mach number. The evaluation of the integral I_4 is carried out in appendix A where it is shown that I_4 can be expressed in terms of complete elliptic integrals of the first and second kinds. Having the expression for I_4, a numerical solution may be obtained for $f_4(x/s\beta)$ (see appendix B). Figure 10 shows a plot of f_4 (a factor representative of the chord lift distribution) for a flat plate wing as a function of $x/s\beta$, the ratio of the distance back from the leading edge to the magnitude of the reduced semispan. The value of f_4 given by equation (25) can be checked in the interval $0 \leq (x/s\beta) \leq 2$ because the exact solution to the complete linearized partial differential equation can be readily obtained there. The comparison is given in figure 10. The fairly rough agreement shown is not surprising since equation (25) is derived on the assumption that the spanwise distribution of load is elliptical at every chord station, and certainly this assumption is least accurate in the interval where the comparison with the exact results is made. The area under the exact and approximate curves in figure 10, between the initial value and that at which $f_4=0$, is nearly the same. (See the next section on Aerodynamic Characteristics.) The integrated value of f_4 as given by equation (25), therefore, can be used for $x/s\beta > 2$.

As for the qualitative nature of the variation, figure 10 shows that the loading on a narrow rectangular wing flying at supersonic speeds falls linearly to zero, becomes negative, and then oscillates between negative and positive values, the amplitude of the oscillation being so heavily damped that after the third change in sign the magnitude is practically zero.

It should be noticed in studying the results of figure 10 that the entire resultant lift of the wing is concentrated in the interval $0 \leq (x/s\beta) \leq 2$. But as the Mach number approaches 1 this interval approaches zero, and the entire lift of the wing is carried in a strip along the leading edge.[6] Such a solution violates, in the vicinity of the leading edge, the assumption on which the theory is based and should be considered only as a theoretical limit.

Results for the lift and pitching moment on the rectangular wing will be developed in a later section.

Subsonic case.—The study of the subsonic rectangular wing stems from equation (16). The first step in the analysis of the equation will be to consider its solution at $\beta s=0$ and show that this is continous with the supersonic results there.

The value of I_2 can be written (equation (15)) as

$$I_2=\int_{-1}^{1}\sqrt{\frac{(x-x_1)^2+\beta^2s^2y^2}{1-y^2}}\,dy$$

and for $\beta s=0$ this becomes

$$I_2=\begin{cases}(x-x_1)\pi & x_1 \leq x\\ -(x-x_1)\pi & x_1 \geq x\end{cases}$$

and hence equation (16) can be written

$$w=\frac{w_0}{c_0}\int_0^x f_2\left(\frac{x_1}{c_0}\right)dx_1 \qquad (36)$$

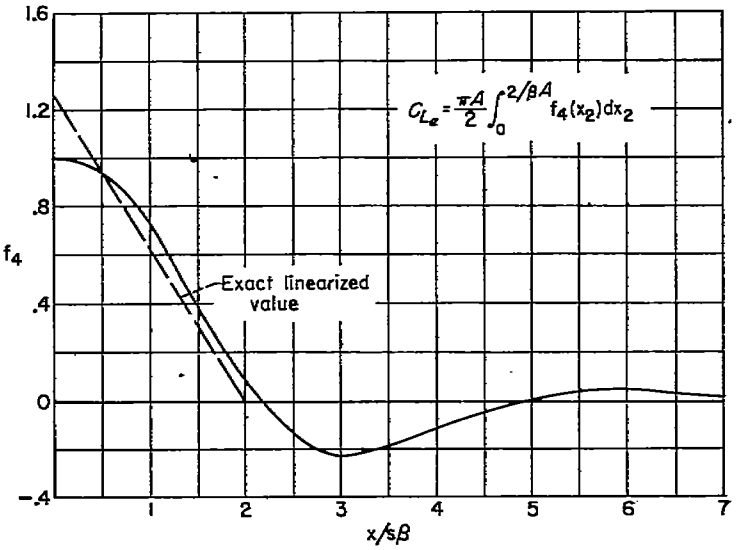

FIGURE 10.—Variation of chordwise correction factor f_4 for supersonic rectangular wing.

[5] The maximum difference in total lift is already less than 6 percent (based on the lower value) and the difference in center of pressure is negligible.

[6] This result also follows by inspecting equation (25) for the values $\beta s=0$.

Equation (36) is identical with the form of the supersonic equation (25) at $\beta s=0$ so that once again the continuity of the subsonic and supersonic theories at the sonic speed range is established. Furthermore, equation (36) shows that if w/w_0 is constant then $f_2(x_0)$ must be zero everywhere except at points where it can be represented by a pulse, the integral of which has a finite magnitude. From the supersonic discussion, it is clear that one such pulse exists and is located at the leading edge.

The evaluation of I_2 for $\beta s>0$ is given in appendix A. The numerical solution to equation (16), assuming the Kutta condition at the trailing edge, is given in appendix B for values of reduced aspect ratio βA equal to 0.33, 1.0, 1.5, and 2.0 For an aspect ratio equal to 2, these values correspond to Mach numbers of 0.986, 0.866, 0.662, and 0, respectively. The results of the computations are shown in figure 11 where the chordwise lift distribution factor $f_2(x_0)$ is plotted against x_0 for the various values of βA. By comparison of figure 11 with figure 10, it can be seen that in the subsonic case the loading drops monotonically from infinity at the leading edge to zero at the trailing edge and does not oscillate in the afterportion, as in the case of the supersonic wing.

When β equals one, these results can be compared with those obtained by Wieghardt and presented in reference 9. Figure 12 shows the comparison for two values of the aspect ratio. Curves are also shown in the figure for the loading obtained by using the method given in appendix B but by satisfying the integral equation at only six and three points. The latter curve is in better agreement with Wieghardt's result and, since Wieghardt (although using a different method involving Birnbaum functions) used only four points, this may account for the discrepancy between the final results of this report and those of Wieghardt.

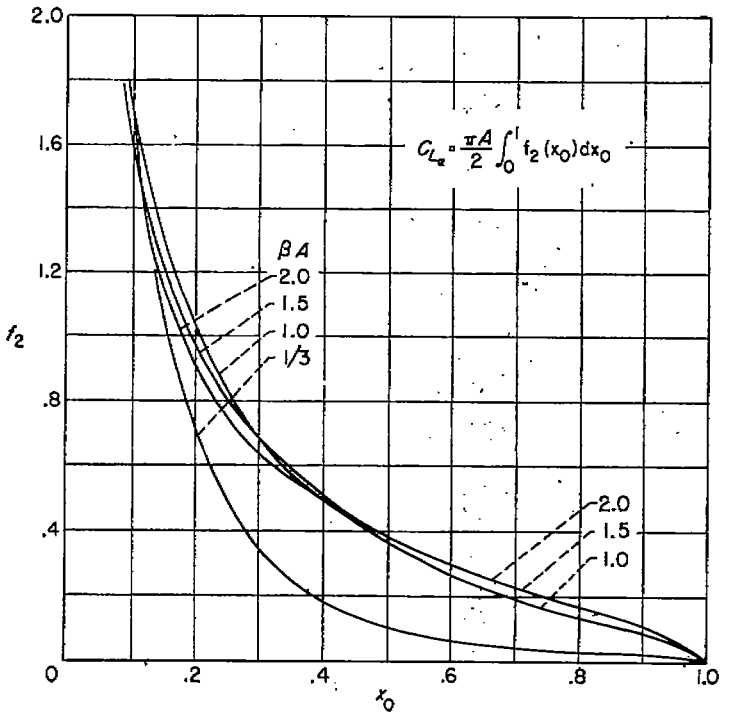

FIGURE 11.—Variation of chordwise correction factor f_2 for subsonic rectangular wing.

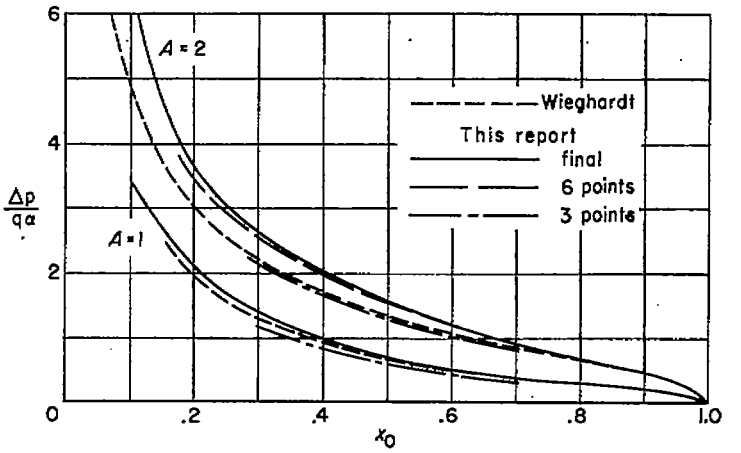

FIGURE 12.—Load distribution along center line of rectangular wing.

AERODYNAMIC CHARACTERISTICS

The previous section presented solutions for the loading on triangular and rectangular wings flying at subsonic and supersonic speeds. This section will be devoted to the conversion of these loadings to expressions for lift and center of pressure.

LIFT

By definition the lift coefficient can be written

$$C_L=\frac{1}{S}\iint_s \frac{\Delta p}{q}\,dx\,dy \tag{37}$$

and this will be evaluated for the various cases for which the loading coefficient has been obtained.

Supersonic triangular wing.—Since the exact linearized value for the loading on the triangular wing flying at supersonic speeds has been derived, the lift coefficient can be written in the form

$$\frac{C_L}{\alpha A}=\frac{\pi}{2E} \tag{38}$$

where A is the aspect ratio and E is the elliptic integral of the second kind with modulus $k=\sqrt{1-\beta^2m^2}$.

Subsonic triangular wing.—In the case of the subsonic triangular wing, equation (37) becomes

$$C_L=\frac{1}{mc_0^2}\int_0^{c_0}dx\int_{-mx}^{mx}\frac{4\alpha m^2x}{\sqrt{m^2x^2-y^2}}f_1\left(\frac{x}{c_0}\right)dy$$

and this becomes (since $A=4m$)

$$\frac{C_L}{\alpha A}=\pi\int_0^1 x_0f_1(x_0)dx_0 \tag{39}$$

The numerical evaluation of equation (39) is not difficult since $x_0f_1(x_0)$ vanishes at $x_0=0$.

Supersonic rectangular wing.—For values of $c_0<2s\beta$ the exact value of the lift coefficient on a rectangular wing flying at supersonic speeds has been obtained and can be written in the form for $\beta A>1$

$$\frac{C_L}{\alpha A}=\frac{4\beta A-2}{(\beta A)^2} \tag{40}$$

When $\beta A<1$ equation (37) must be used in connection with equation (24) and there results

$$C_L=\frac{1}{2sc_0}\int_0^{c_0}dx\int_{-s}^{s}\frac{4\alpha}{s\beta}f_4\left(\frac{x}{s\beta}\right)\sqrt{s^2-y^2}\,dy$$

which reduces to

$$C_L=\frac{\alpha\pi}{c_0\beta}\int_0^{c_0}f_4\left(\frac{x}{s\beta}\right)dx$$

and this can be written in the form

$$\frac{C_L}{\alpha A}=\frac{\pi}{\beta A c_0}\int_0^{c_0}f_4\left(\frac{2x}{c_0\beta A}\right)dx$$

which becomes, if $x_2=\frac{2x}{c_0\beta A}$,

for $\beta A<1$

$$\frac{C_L}{\alpha A}=\frac{\pi}{2}\int_0^{\frac{2}{\beta A}}f_4(x_2)dx_2 \tag{41}$$

Subsonic rectangular wing.—The equation for the loading on a subsonic rectangular wing, equation (14), placed in the formula for lift coefficient yields

$$C_L=\frac{1}{2sc_0}\int_0^{c_0}dx\int_{-s}^{s}\frac{4\alpha}{c_0}f_2\left(\frac{x}{c_0}\right)\sqrt{s^2-y^2}\,dy$$

which becomes

$$\frac{C_L}{\alpha A}=\frac{\pi}{2}\int_0^1 f_2(x_0)dx_0 \tag{42}$$

The evaluation of equation (42) by numerical means requires special consideration since $f_2(x_0)$ approaches infinity at the leading edge as shown in figure 11. To this end, rewrite equation (42) in the form

$$\frac{C_L}{\alpha A}=\frac{\pi}{2}\int_0^{\epsilon}f_2(x_0)dx_0+\frac{\pi}{2}\int_{\epsilon}^1 f_2(x_0)dx_0 \tag{43}$$

and equation (B4) in the appendix (for the special case in which $x_0=1$) in the form

$$1=\frac{1}{2\pi}\int_0^{\epsilon}f_2(x_0)\left[\pi+\frac{\beta AE}{k(1-x_0)}\right]dx_0+\frac{1}{2\pi}\int_{\epsilon}^1 f_2(x_0)\left[\pi+\frac{\beta AE}{k(1-x_0)}\right]dx_0 \tag{44}$$

An application of the mean-value theorem yields

$$\int_0^{\epsilon}f_2(x_0)dx_0=\frac{1}{\left[\pi+\frac{\beta AE_\theta}{k_\theta(1-\theta)}\right]}\left\{2\pi-\int_{\epsilon}^1 f_2(x_0)\left[\pi+\frac{\beta AE}{k(1-x_0)}\right]dx_0\right\} \tag{45}$$

where E_θ has the modulus k_θ which equals $\beta A/\sqrt{4(1-\theta^2)+(\beta A)^2}$ and where $0<\theta<\epsilon$. The combination of equations (43) and (45) yields an expression for the lift coefficient involving only the load distribution from a distance ϵ/c_0 back of the leading edge to the trailing edge.

PITCHING MOMENT

By definition the pitching-moment coefficient about the apex or leading edge and based on the root chord can be written

$$C_m=-\frac{1}{Sc_0}\int\int_S x\frac{\Delta p}{q}dx\,dy \tag{46}$$

Equation (46) will be applied to the various loadings which have been studied.

Supersonic triangular wing.—The exact linearized value for the pitching-moment coefficient on a triangular wing flying at supersonic speeds has been derived elsewhere and can be written in the form

$$\frac{C_m}{\alpha A}=-\frac{\pi}{3E} \tag{47}$$

Subsonic triangular wing.—The derivation of the pitching moment on a subsonic triangular wing proceeds in the same manner as the derivation of lift and there results

$$\frac{C_m}{\alpha A}=-\pi\int_0^1 x_0^2 f_1(x_0)dx_0 \tag{48}$$

This expression can be easily integrated numerically.

Supersonic rectangular wing.—For values of βA greater than 1 the pitching-moment coefficient on a rectangular wing is given by the equation, for $\beta A>1$

$$\frac{C_m}{\alpha A}=-\frac{6\beta A-4}{3(\beta A)^2} \tag{49}$$

When $\beta A<1$ the solution to the integral equation must be used and the final expression can be written

$$\frac{C_m}{\alpha A}=-\frac{\pi\beta A}{4}\int_0^{\frac{2}{\beta A}}x_2 f_4(x_2)dx_2 \tag{50}$$

Subsonic rectangular wing.—The equation for the pitching-moment coefficient on a subsonic rectangular wing follows in the same manner as did that for the lift coefficient. Hence,

$$\frac{C_m}{\alpha A}=-\frac{\pi}{2}\int_0^1 x_0 f_2(x_0)dx_0 \tag{51}$$

and, since the variation of $x_0 f_2(x_0)$ is as indicated in figure 13 the numerical integration of equation (51) is simple.

CENTER OF PRESSURE

Since the pitching moment is based on the root chord, the center of pressure of all wing plan forms can be written

$$\frac{x_{c.p.}}{c_0}=\frac{C_m}{C_L} \tag{52}$$

DISCUSSION OF RESULTS

Figures 14 and 15 show the variation of the lift coefficient and center of pressure on triangular and rectangualr wings for values of βA between zero and 2. For the triangular wing, the differences between the subsonic and supersonic cases are not large in this interval of reduced aspect ratio; the subsonic wing develops somewhat less lift and its center of pressure moves forward as βA increases. The characteristics of the rectangular wing, however, show a large variation in passing through the speed of sound.

The subsonic rectangular wing has a variation of $C_L/A\alpha$ with $A\beta$ which is almost identical with that for the subsonic

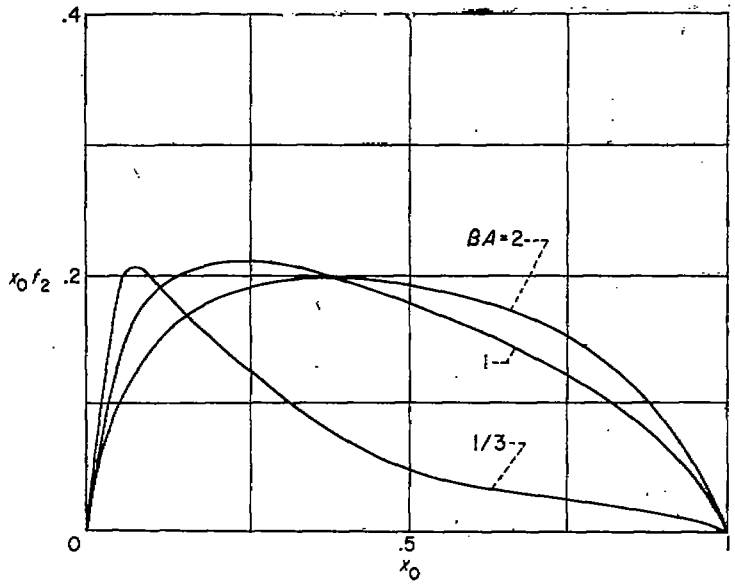

FIGURE 13.—Variation of $x_0 f_2$ with x_0.

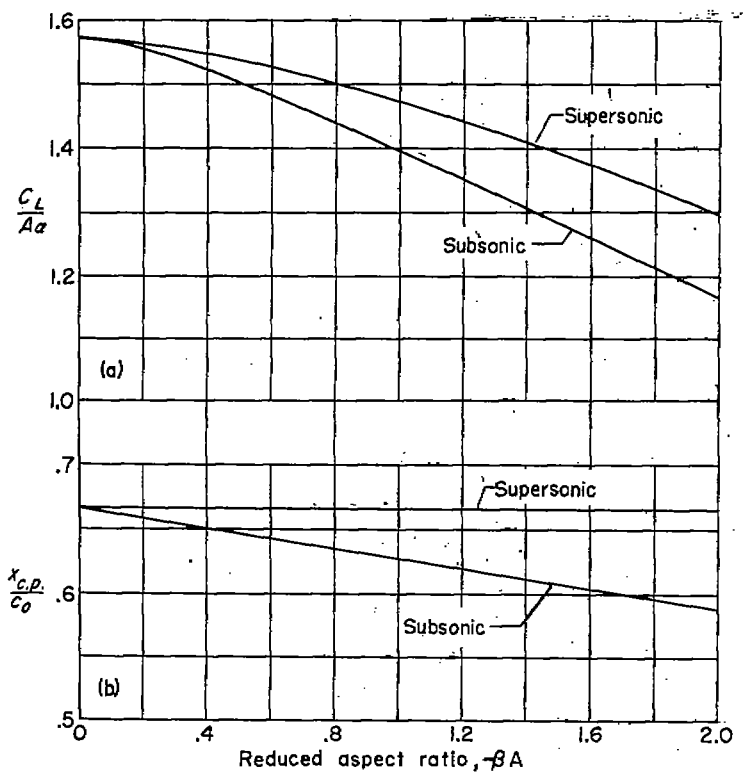

(a) Lift.
(b) Center of pressure.

FIGURE 14.—Aerodynamic characteristics of a triangular wing having a low value of βA.

triangular wing. Unlike the triangular wing, however, the curve for $x_{c.p.}/c_0$ on the rectangular wing shows this lift to be carried farther and farther forward with decreasing βA, from the quarter-chord position at $\beta A = \infty$ all the way to the leading edge at $\beta A = 0$.

As the speed is further increased and the rectangular wing enters the supersonic speed range, the magnitude of the lift begins to oscillate with increasing amplitude. This continues until the reduced aspect ratio rises to one, after which, as

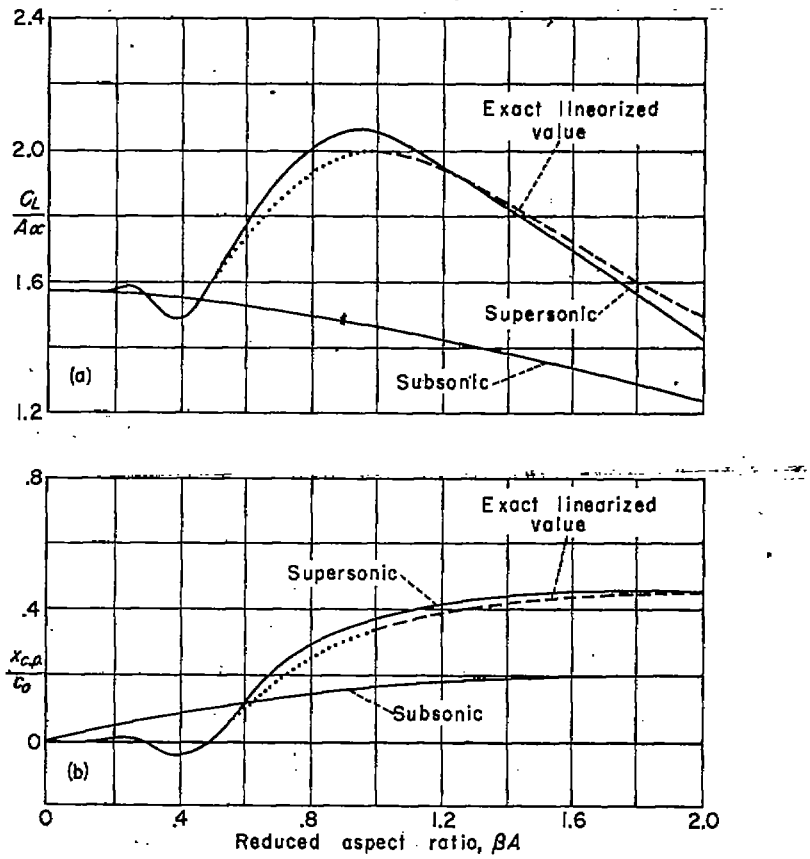

(a) Lift.
(b) Center of pressure.

FIGURE 15.—Aerodynamic characteristics of rectangular wing having a low value of βA.

βA increases still farther, the value of $C_L/A\alpha$ falls uniformly to zero according to the expression

$$\frac{C_L}{A\alpha} = \frac{4}{\beta A}\left(1 - \frac{1}{2\beta A}\right), \qquad \beta A \geq 1 \tag{53}$$

which is the exact equation for the lift coefficient given by linearized lifting-surface theory. The difference between the values of lift coefficient given by equations (41) and (53), represented in figure 15 by the solid and dashed lines, respectively, has already been discussed in the section on loading; the approximate solution is based on the assumption that the span loading at each chord station is elliptical and such an assumption is increasingly unrealistic for increasing βA. The dotted line shown in the figure appears to be a reasonable interpolation between $\beta A = 1$, the lower limit to which equation (53) applies, and a point where the approximate solution given by equation (41) can be considered trustworthy.

The variation of the center of pressure on a supersonic rectangular wing indicates that the wing is unstable for all positions of the pivot point behind the leading edge for values of βA around 0.4, the center of pressure, in such a range, having moved forward of the wing leading edge. As βA increases past the value of 0.5, however, the center of pressure moves back along the wing and rapidly approaches the midchord point, its location for a wing of infinite aspect ratio.

COMPARISON OF RESULTS FOR SUBSONIC TRIANGULAR WINGS WITH OTHER THEORIES AND SOME EXPERIMENTS

DISCUSSION OF THE THEORETICAL RESULTS

Several other published theories can be used to calculate the forces and moments on low-aspect-ratio triangular wings flying at subsonic speeds. A comparison between values of C_{L_α} and center of pressure given by those theories and by the method of this report is summarized in figure 16.

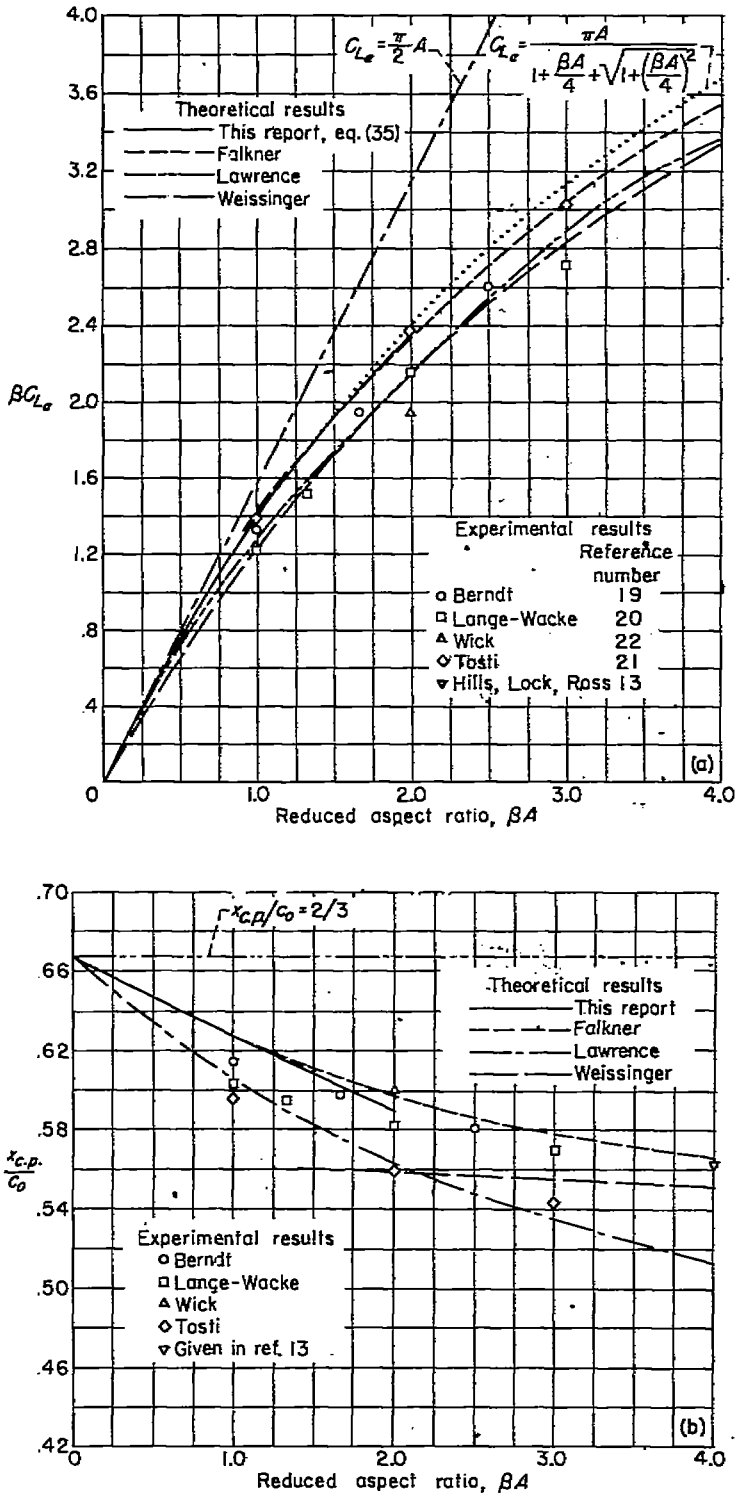

(a) Lift.
(b) Center of pressure.

FIGURE 16.—Various theoretical and experimental results for triangular wings showing the variation of βC_{L_α} and $x_{c.p.}/c_0$ with reduced aspect ratio, βA.

The theories of Falkner (reference 13) and Weissinger (reference 14) are well known and will not be discussed in detail here. The results obtained from Weissinger's method were presented by De Young and Harper in reference 15 for aspect ratios equal to 1.5, 2.5, and 3.5; those obtained from Falkner's method were presented by Berndt in reference 16 for aspect ratios equal to 1.0, 1.67, and 2.5, and by Falkner in reference 13 for an aspect ratio equal to 4. Both Berndt and Falkner used 126 vortices and 6 control points so the accuracy of their calculations is similar. It should be mentioned, however, that in order to make Berndt's results consistent with Falkner's, the values of C_{L_α} given by Berndt have been multiplied by a factor [7] suggested and used by Falkner in reference 13.

The results shown for Lawrence's theory were presented in reference 17 and are based on a method originally given in reference 18.

The differences between values obtained from each of the theories can be attributed to differences in the various simplifying assumptions used. The Weissinger and Lawrence theories agree on values of C_{L_α} but disagree as to the position of the center of pressure. Falkner's method and the method of this report yield results in good agreement for both C_{L_α} and center-of-pressure location. However, for $\beta A=2$, the Weissinger-Lawrence value of C_{L_α} is about 9 percent below and the center-of-pressure position about 3 percent (based on the root chord) farther forward than similar values obtained in this report [8] or by Falkner's method.

DISCUSSION OF THE EXPERIMENTAL DATA

Experimental data for low-aspect-ratio triangular wings are given in references 13 and 19 through 22. The sections, aspect-ratio range, Reynolds numbers (based on the mean aerodynamic chord), and section thickness ratios are given in table III.

The source of the experimental values for the $A=4$ wing (given in reference 13) is some unpublished British wind-tunnel data. The Reynolds number is given as "high" and the section is not specified. Reference 21 presents the results of experiments made in the Langley free-flight tunnel on some flat-plate (¼ inch thick with rounded leading edge) models having beveled trailing edges. Hence, the values for the thickness ratios listed for these tests are effective thickness ratios, being, in fact, the plate thickness divided by the root mean chord of the wing, $(2/3)c_0$.

The experimental data presented in table IV are portions of the data given in references 19 and 20 and the values shown in figure 16 were obtained from curves constructed by means of these numbers. Reference 21 presents experimental results in graphical form and the slopes used in figure 16 were read from these graphs. It should be mentioned that reference 21 also gives results for an aspect ratio 0.5 wing but the data presented are not sufficient to

[7] According to Falkner (reference 13): "It has not been possible to establish the factor for all cases, but figures derived from a delta and other wings suggest that the factor can be taken tentatively as independent of aspect ratio, and to vary as $1+0.029$ (tangent of sweepback of quarter chord)."

[8] It can be shown, however, that the integral equation used by Lawrence to obtain the curves shown in figure 16 and the one used in this report both approach the same values of C_{L_α} and $x_{c.p.}/c_0$ as the angle of sweep goes to either $\pi/2$ or zero. In the former case they approach the familiar Jones' low-aspect-ratio-theory results, and in the latter case they yield 3π for C_{L_α} and 1/3 for $x_{c.p.}/c_0$.

fix the slopes of the lift and moment curves near zero angle of attack. Hence, no values for this aspect ratio are presented. Finally, the values taken from reference 22 were read from graphs presented therein and based on integrated pressure distributions (measurements taken along five span stations).

COMPARISON OF EXPERIMENT WITH THEORY—LIFT-CURVE SLOPE

The experimental data shown in figure 16 (a) do not seem at first glance to favor either group of theories. However, since all these theories are based on the assumption of zero thickness, it is pertinent to examine the data on the basis of thickness ratio. A correlation on this basis is presented in figure 17. It shows that with decreasing thickness ratio, the ratio of the experimental values to those predicted by the method of this report (in the range $0 \leq \beta A \leq 2$) or by Falkner's method (in the range $2 \leq \beta A \leq 4$) tends to unity. Of course, this trend is not conclusively borne out by these comparisons and should be tested by more experimental measurements in the lower thickness ratio range.

It is interesting to notice that a good approximation to the results calculated in this report and by Falkner's method is given by the equation

$$C_{L_\alpha}=\frac{2\pi A}{pA+2} \qquad (54)$$

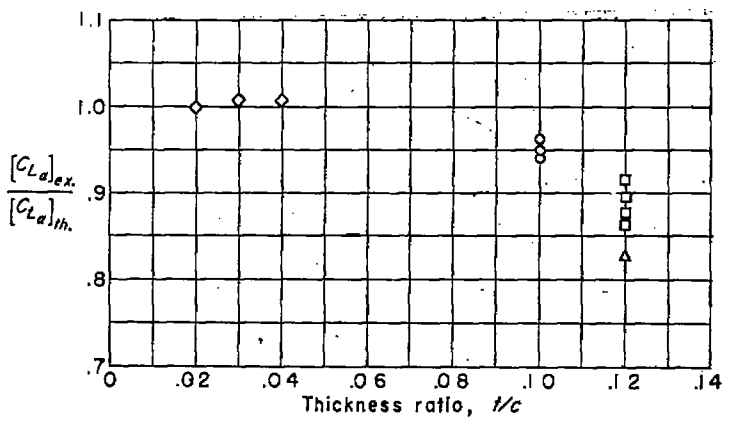

FIGURE 17.—Variation of $(C_{L_\alpha})_{ex.}/(C_{L_\alpha})_{th.}$, the ratio of the measured lift-curve slope to that given by the theoretical methods of Falkner or this report with thickness ratio.

where

$$p=\frac{\text{wing semiperimeter}}{\text{wing span}}$$

Equation (54) was derived by R. T. Jones (see reference 23) as a first-order correction to the value of C_{L_α} given by lifting-line theory for wings having elliptic plan forms. It has been found, however, to provide a good estimate for the aspect-ratio correction to wings of various plan forms.[9] For the particular case of the triangular wing in compressible flow, equation (54) becomes

$$\beta C_{L_\alpha}=\frac{\pi\beta A}{1+\frac{\beta A}{4}+\sqrt{1+\left(\frac{\beta A}{4}\right)^2}} \qquad (55)$$

and its variation for $0 \leq \beta A \leq 4$ is shown in figure 16 (a).

COMPARISON OF EXPERIMENT WITH THEORY—CENTER-OF-PRESSURE LOCATION

The comparison between experimental and theoretical values of center-of-pressure location is shown in figure 16 (b). In weighting the experimental points shown, it should be remembered that the tests recorded in reference 21 were made on a flat plate with a beveled trailing edge. When such a wing is at a positive angle of attack, the bevel causes the flow to separate at the surface discontinuity producing an effective upwardly deflected flap. The result is a loss of lift on the rearward portion of the wing and a forward shift in center of pressure. Hence, the experimental values for $x_{c.p.}/c_0$ taken from reference 21 should be low relative to the values given in the other references. With this taken into consideration, the experimental values shown in figure 16 (b) are in fairly good agreement and again favor, at least, the theoretical results based on Falkner's method.

AMES AERONAUTICAL LABORATORY
NATIONAL ADVISORY COMMITTEE FOR AERONAUTICS
MOFFETT FIELD, CALIF., *Nov. 28, 1952.*

[9] This approximation is suggested in an article by R. T. Jones and Doris Cohen, "Aerodynamics of Wings at High Speed," to be published by the Princeton University Press in section A of the book entitled Applied High-Speed Aerodynamics, volume VI of the High-Speed Aerodynamics and Jet Propulsion Series.

APPENDIX A

EVALUATION OF SPECIAL INTEGRALS

THE INTEGRAL I_1

The evaluation of I_1 will be discussed first for the case in which $x>x_1$ and second for the case in which $x<x_1$.

CASE 1, $x>x_1$

It is possible to write I_1 in the form

$$I_1=\int_{\mu_0}^{\mu_1}\frac{\sqrt{\mu_0^2+\beta^2m^2\eta^2}}{\eta\sqrt{(\eta-\mu_0)(\mu_1-\eta)}}\,d\eta \tag{A1}$$

where $\mu_0=m(x-x_1)$ and $\mu_1=m(x+x_1)$. The linear term in the lower radical of the integrand can be eliminated by the transformation $\eta=(\sigma+\delta t)/(1+t)$, and the integral becomes

$$I_1=\frac{\delta-\sigma}{\sqrt{(\mu_0-\sigma)(\sigma-\mu_1)}}\int_{\frac{\sigma-\mu_0}{\mu_0-\delta}}^{\frac{\sigma-\mu_1}{\mu_1-\delta}}\frac{\sqrt{(\mu_0^2+\sigma^2\beta^2m^2)+(\mu_0^2+\delta^2\beta^2m^2)t^2}}{(1+t)(\sigma+\delta t)\sqrt{1-\left(\frac{\mu_1-\delta}{\sigma-\mu_1}\right)\left(\frac{\delta-\mu_0}{\beta-\mu_0}\right)t^2}}\,dt \tag{A2}$$

where

$$\sigma=\frac{-\mu_0(\mu_0-\beta^2m^2\mu_1)+\mu_0\sqrt{(1+\beta^2m^2)(\mu_0^2+\beta^2m^2\mu_1^2)}}{\beta^2m^2(\mu_1+\mu_0)} \tag{A3}$$

and

$$\delta=\frac{-\mu_0(\mu_0-\beta^2m^2\mu_1)-\mu_0\sqrt{(1+\beta^2m^2)(\mu_0^2+\beta^2m^2\mu_1^2)}}{\beta^2m^2(\mu_1+\mu_0)} \tag{A4}$$

The expression for σ and δ may be combined to give the useful identities

$$\mu_0^2=-\sigma\delta\beta^2m^2$$

$$(\mu_0-\sigma)(\delta-\mu_1)+(\mu_1-\sigma)(\delta-\mu_0)=0$$

Using fundamental properties of even and odd functions, equation (A2) may be reduced to the form

$$I_1=2\sqrt{\frac{\mu_0^2+\sigma^2\beta^2m^2}{(\mu_1-\delta)(\mu_0-\delta)}}\int_0^1\left[\left(\frac{1}{1+\frac{\sigma k^2}{\delta k'^2}\omega^2}-\frac{\delta/\sigma}{1+\frac{\delta k^2}{\sigma k'^2}\omega^2}\right)\frac{1}{k'}\sqrt{\frac{k'^2+k^2\omega^2}{1-\omega^2}}\right]d\omega$$

by the substitution

$$\omega=\left|\frac{\mu_1-\delta}{\mu_1-\sigma}\right|t$$

and where

$$k^2=\frac{(\mu_1-\sigma)^2\delta}{(\mu_1^2-\sigma\delta)(\delta-\sigma)}$$

$$\frac{k^2}{k'^2}=-\frac{\delta}{\sigma}\left(\frac{\mu_1-\sigma}{\mu_1-\delta}\right)^2$$

By introducing the Jacobian elliptic functions in the transformations $\omega=cnu$, the integral reduces to

$$I_1=\frac{2}{k}\sqrt{\frac{\mu_0^2+\delta^2\beta^2m^2}{(\mu_1-\sigma)(\sigma-\mu_0)}}\int_0^K\left(\frac{\nu_1^2}{1+\nu_1^2sn^2u}-\frac{\frac{\sigma}{\delta}\nu_2^2}{1+\nu_2^2sn^2u}\right)dn^2u\,du \tag{A5}$$

where

$$\nu_1^2=\frac{-\left(\frac{\sigma}{\delta}\right)k^2}{k'^2+\frac{\sigma}{\delta}k^2}>0 \tag{A6}$$

and

$$\nu_2^2=\frac{-\left(\frac{\delta}{\sigma}\right)k^2}{k'^2+\frac{\delta}{\sigma}k^2}>0 \tag{A7}$$

The integration may now be completed and

$$I_1=\frac{2}{k}\sqrt{\frac{\mu_0^2+\delta^2\beta^2m^2}{(\mu_1-\sigma)(\sigma-\mu_0)}}\left[\nu_1\sqrt{\frac{\nu_1^2+k^2}{1+\nu_1^2}}\,G\left(\frac{\nu_1}{\sqrt{\nu^2+k^2}}\right)-\frac{\sigma}{\delta}\nu_2\sqrt{\frac{\nu_2^2+k^2}{1+\nu_2^2}}\,G\left(\frac{\nu_2}{\sqrt{\nu_2^2+k^2}}\right)\right]$$

$$=2\left[\beta mG\left(\frac{\nu_1}{\sqrt{\nu_1^2+k^2}}\right)+\sqrt{\frac{\mu_0}{\mu_1}}\,G\left(\frac{\nu_2}{\sqrt{\nu_2^2+k^2}}\right)\right] \tag{A8}$$

where

$$G(x)=EF'(x)+KE'(x)-KF'(x) \tag{A9}$$

the modulus of the elliptic integrals being k or k'.

CASE 2, $x<x_1$

The procedure for obtaining the solution for I_1 in this case is identical to that followed in case 1 except that in order to fulfill the contition that $t>-1$, σ and δ must be defined in the following manner

$$\delta=\frac{-\mu_0(\mu_0-\beta^2m^2\mu_1)+\mu_0\sqrt{(1+\beta^2m^2)(\mu_0^2+\beta^2m^2\mu_1^2)}}{\beta^2m^2(\mu_1+\mu_0)} \tag{A10}$$

$$\sigma=\frac{-\mu_0(\mu_0-\beta^2m^2\mu_1)-\mu_0\sqrt{(1+\beta^2m^2)(\mu_0^2+\beta^2m^2\mu_1^2)}}{\beta^2m^2(\mu_1+\mu_0)} \tag{A11}$$

In this case it can be shown that in equation (A5) $\nu_1>0$ and $\nu_2<-1$, and the solution for I_1 is

$$I_1=2\left\{\beta m G\left(\frac{\nu_1}{\sqrt{\nu_1^2+k^2}}\right)+\beta m\sqrt{\frac{\delta\sigma}{\mu_0\mu_1}}\left[KE\left(\frac{-1}{\nu_2}\right)-EF\left(\frac{-1}{\nu_2}\right)\right]+\frac{\sigma}{\delta}k\sqrt{\frac{\mu_0^2+\delta^2\beta^2m^2}{(\mu_1-\sigma)(\sigma-\mu_0)}}K\right\} \quad (A12)$$

where $G(x)$ is defined as in equation (A9).

THE INTEGRAL I_2

Writing I_2 in the form

$$I_2=2\int_0^s\sqrt{\frac{(x-x_1)^2+y_1^2\beta^2}{s^2-y_1^2}}dy_1 \quad (A13)$$

and setting

$$\frac{y_1}{s}=cnu,\ k=\frac{\beta s}{\sqrt{(x-x_1)^2+\beta^2s^2}}$$

I_2 can be integrated to give

$$I_2=2\beta s\int_0^K\frac{dn^2u\,du}{k}=\frac{2\beta sE}{k} \quad (A14)$$

THE INTEGRAL I_3

CASE 1, $\theta_0\mu_1<\mu_0<\mu_1$

Writing I_3 in the form

$$I_3=\theta_0\int_{\mu_0}^{\mu_1}\frac{d\eta}{\eta}\sqrt{\frac{\frac{\mu_0^2}{\theta_0^2}-\eta^2}{(\mu_1-\eta)(\eta-\mu_0)}} \quad (A15)$$

and making the transformation

$$sn^2u=\frac{2}{(1-\theta_0^2)k^2}\frac{\eta-\mu_0}{\eta+\frac{\mu_0}{\theta_0}} \quad (A16)$$

where

$$k^2=\frac{2\theta_0}{1-\theta_0}\frac{\mu_1-\mu_0}{\mu_1\theta_0+\mu_0} \quad (A17)$$

reduces equation (A15) to the form

$$I_3=(1+\theta_0)k\sqrt{\frac{2\mu_0}{\theta_0(\mu_1-\mu_0)}}\left(\int_0^K\frac{du}{1+\frac{1-\theta_0}{2\theta_0}k^2sn^2u}-\int_0^K\frac{\theta_0du}{1-\frac{1-\theta_0}{2}k^2sn^2u}\right)$$

The integration may now be completed and

$$I_3=\sqrt{\frac{2\mu_0\theta_0}{\mu_1-\mu_0}}k\left\{(1-\theta_0)K+\frac{\sqrt{1-\theta_0^2}\,G\left(\sqrt{\frac{1-\theta_0}{1+\theta_0}}\right)}{\theta_0\sqrt{1+\frac{1-\theta_0}{2\theta_0}k^2}}-\frac{\sqrt{1-\theta_0^2}}{\sqrt{1-\frac{1-\theta_0}{2}k^2}}\left[KE\left(\sqrt{\frac{1-\theta_0}{2}}\right)-EF\left(\sqrt{\frac{1-\theta_0}{2}}\right)\right]\right\} \quad (A18)$$

CASE 2, $0<\mu_0<\theta_0\mu_1$

In this case

$$I_3=\theta_0\int_{\mu_0}^{\frac{\mu_0}{\theta_0}}\sqrt{\frac{\frac{\mu_0^2}{\theta_0^2}-\eta^2}{(\mu_1-\eta)(\eta-\mu_0)}}\frac{d\eta}{\eta} \quad (A19)$$

and the transformation

$$sn^2u=\frac{2}{1-\theta_0}\frac{\eta-\mu_0}{\eta+\frac{\mu_0}{\theta_0}}$$

is made where

$$k^2=\frac{1-\theta_0}{2}\frac{\mu_1+\frac{\mu_0}{\theta_0}}{\mu_1-\mu_0}$$

Equation (A19) then becomes

$$I_3=(1+\theta_0)\sqrt{\frac{2\mu_0}{\theta_0(\mu_1-\mu_0)}}\left(\int_0^K\frac{du}{1+\frac{1-\theta_0}{2\theta_0}sn^2u}-\int_0^K\frac{\theta_0du}{1-\frac{1-\theta_0}{2}sn^2u}\right)$$

The integration can be completed so that

$$I_3=(1+\theta_0)\sqrt{\frac{2\mu_0}{\theta_0(\mu_1-\mu_0)}}\left\{\theta_0K\left(\frac{2k^2}{1-\theta_0+2\theta_0k^2}-1\right)+\sqrt{\frac{2\theta_0(1-\theta_0^2)}{1-\theta_0+2\theta_0k^2}}\frac{G\left(\sqrt{\frac{1-\theta_0}{1-\theta_0+2\theta_0k^2}}\right)}{1+\theta_0}-\frac{\theta_0}{1+\theta_0}\sqrt{\frac{2(1-\theta_0^2)}{2k^2-1+\theta_0}}\left[KE\left(\frac{1}{k}\sqrt{\frac{1-\theta_0}{2}}\right)-EF\left(\frac{1}{k}\sqrt{\frac{1-\theta_0}{2}}\right)\right]\right\} \quad (A20)$$

THE INTEGRAL I_4

CASE 1, $0\le X_1\le X-\beta s$

The integral I_4 can be written

$$I_4=2\int_0^s\sqrt{\frac{(x-x_1)^2-\beta^2y_1^2}{s^2-y_1^2}}\,dy_1 \quad (A21)$$

When the transformation $snu=y_1/s$ is made, the expression may be integrated to give

$$I_4=2(x-x_1)\int_0^K dn^2u\,du=2(x-x_1)E_1 \quad (A22)$$

where

$$k_1^2=\frac{s^2\beta^2}{(x-x_1)^2} \quad (A23)$$

CASE 2, $X-\beta s\le X_1\le X$

In this case I_4 can be written

$$I_4=2\int_0^{\frac{x-x_1}{\beta}}\sqrt{\frac{(x-x_1)^2-\beta^2y_1^2}{s^2-y_1^2}}\,dy_1 \quad (A24)$$

The transformation $snu=\beta y_1/(x-x_1)$ applied to equation (A24) yields

$$I_4=2\int_0^K\frac{(x-x_1)^2}{\beta s}cn^2u\,du=2k_2(x-x_1)B_2 \quad (A25)$$

where

$$k_2=\frac{x-x_1}{\beta s} \quad (A26)$$

and

$$B_2=\frac{E_2-k_2'^2K_2}{k_2^2} \quad (A27)$$

APPENDIX B

NUMERICAL SOLUTION OF INTEGRAL EQUATIONS

SUBSONIC TRIANGULAR WING

Since the integral I_1 is a function only of the ratio x_1/x, equation (10) can be written for $\overline{w}=w_0$

$$1=\frac{1}{2}\int_0^1 \frac{\xi f_1(x\xi/c_0)d\xi}{\sqrt{1-\xi^2}}+\frac{1}{2\pi}\int_0^{c_0/x}\frac{\xi}{1-\xi}I_1(\xi)f_1(x\xi/c_0)d\xi \qquad \text{(B1)}$$

where $\xi=x_1/x$. It is now assumed that $f_1(x\xi/c_0)$ may be considered constant over small intervals. This reduces the solution of the integral equation to the elementary problem of solving a system of simultaneous algebraic equations. On the basis of such an assumption, equation (B1) becomes

$$1=\frac{1}{2\pi}\sum_{i=1}^{n} f_1\left(\frac{2i-1}{2n}\right)\int_{\frac{2(i-1)}{2i-1}}^{\frac{2i}{2i-1}} g_0(\xi)d\xi; \quad j=1,2,3,\ldots n \qquad \text{(B2)}$$

where

$$\left.\begin{aligned} g_0(\xi)&=\frac{\pi\xi}{\sqrt{1-\xi^2}}+\frac{\xi}{1-\xi}I_1(\xi); \quad 0\le\xi\le 1\\ g_0(\xi)&=\frac{\xi}{1-\xi}I_1(\xi); \quad 1\le\xi\le\frac{c_0}{x}\end{aligned}\right\} \qquad \text{(B3)}$$

The function $g_0(\xi)$ was calculated by numerical integration and systems of simultaneous equations were obtained for values of n equal to 3, 6, and 9. Solutions were found using the Gauss-Seidel method (for which the simultaneous equations were well suited).

SUBSONIC RECTANGULAR WING

Substituting the value of I_2 given by equation (A14) into equation (16), one has for $w=w_0$

$$1=\frac{1}{2\pi}\int_0^1 g\left(\frac{x-x_1}{c_0}\right)f_2\left(\frac{x_1}{c_0}\right)d\left(\frac{x_1}{c_0}\right) \qquad \text{(B4)}$$

where

$$g\left(\frac{x-x_1}{c_0}\right)=\pi+\frac{\beta AE}{\left(\frac{x-x_1}{c_0}\right)k}$$

and where

$$k=\frac{\beta s}{\sqrt{(x-x_1)^2+\beta^2s^2}}=\frac{\beta A}{\sqrt{4\left(\frac{x-x_1}{c_0}\right)^2+\beta^2A^2}}$$

A satisfactory numerical solution of equation (B4) requires the solution of the system of simultaneous equations of the form

$$1=\frac{1}{2\pi}\sum_{i=1}^{n}\frac{1}{2n}\left\{f_2(0)g\left(\frac{2i-1}{2n}-0\right)+2\left[f_2\left(\frac{1}{n}\right)g\left(\frac{2i-1}{2n}-\frac{1}{n}\right)+\right.\right.$$
$$\left.\left.f_2\left(\frac{2}{n}\right)g\left(\frac{2i-1}{2n}-\frac{2}{n}\right)+\ldots+f_2\left(\frac{n-1}{n}\right)g\left(\frac{2i-1}{2n}-\frac{n-1}{n}\right)\right]+$$
$$f_2(1)g\left(\frac{2i-1}{2n}-1\right)\right\} \qquad \text{(B5)}$$

The convergence of the solutions to equation (B5) is indicated in figure 18 where the value of n was successively taken to be 3, 6, and 9.

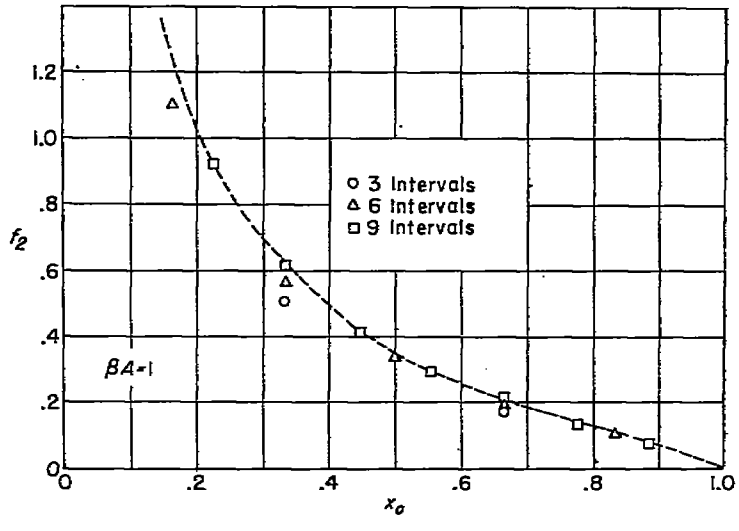

FIGURE 18.—Solutions obtained for the variation of f_2 with x_0 using 3, 6, and 9 intervals in equation (B5).

SUPERSONIC RECTANGULAR WING

Equation (25) can be written when $w=w_0$ as

$$1=f_4\left(\frac{x}{s\beta}\right)+\int_0^x g_1\left(\frac{x-x_1}{s\beta}\right)f_4\left(\frac{x_1}{s\beta}\right)\frac{dx_1}{s\beta} \qquad \text{(B6)}$$

where from equations (A22) and (A25)

$$g_1\left(\frac{x-x_1}{s\beta}\right)=\left\{\begin{aligned}&\frac{2}{\pi}E_1 \quad \frac{x-x_1}{\beta s}\ge 1\\ &\frac{2}{\pi}k_2B_2\,\frac{x-x_1}{\beta s}\le 1\end{aligned}\right\} \qquad \text{(B7)}$$

and where

$$k_1=\frac{s\beta}{x-x_1} \qquad k_2=\frac{x-x_1}{s\beta}$$

By the application of the trapezoidal rule for numerical integration to equation (B6), it is possible to write $f_4(x/s\beta)$ explicitly as

$$f_4\left(\frac{x}{\beta s}\right)=1-\frac{1}{2}\Delta\left(\frac{x}{\beta s}\right)\left[g_1(0)+2\sum_{i=1}^{n}g_1\left(\frac{x}{\beta s}\right)_i f\left(\frac{x}{\beta s}\right)_i\right] \qquad \text{(B8)}$$

where $\Delta(x/\beta s)$ is the interval of the trapezoid.

APPENDIX C

EVALUATION OF δ

Consider the integral equation

$$2\pi x_0=\int_0^{x_0}\frac{\pi x_2 f_1(x_2)\,dx_2}{\sqrt{x_0^2-x_2^2}}+\int_1^{1}\frac{x_2 I_1\left(\frac{x_2}{x_0}\right)f_1(x_2)\,dx_2}{x_0-x_2} \quad \text{(C1)}$$

In order to study $f_1(x_2)$ in the neighborhood of the origin, first set $x_2=x_0\xi$ so that equation (C1) becomes

$$2\pi=\int_0^1\frac{\pi\xi f_1(x_0\xi)\,d\xi}{\sqrt{1-\xi^2}}+\int_0^{1/x_0}\frac{\xi I_1(\xi)f_1(x_0\xi)\,d\xi}{1-\xi} \quad \text{(C2)}$$

then assume that, for small values of x_2, $f_1(x_2)$ can be expressed as

$$f_1(x_2)\sim\frac{a_0}{x_2^{\delta}}$$

From this one has

$$2\pi=\lim_{x_0\to 0}\frac{a_0}{x_0^{\delta}}\left[\pi\int_0^1\frac{\xi^{1-\delta}d\xi}{\sqrt{1-\xi^2}}+\int_0^{1/x_0}\frac{\xi^{1-\delta}I_1(\xi)\,d\xi}{1-\xi}\right] \quad \text{(C3)}$$

which immediately implies

$$\pi\int_0^1\frac{\xi^{1-\delta}d\xi}{\sqrt{1-\xi^2}}+\int_0^{\infty}\frac{\xi^{1-\delta}I_1(\xi)\,d\xi}{1-\xi}=0 \quad \text{(C4)}$$

The value of δ in the interval $0\leq\beta A<2$ that satisfies equation (C4) was determined by numerical integration. The results are shown in figure 8.

REFERENCES

1. Jones, Robert T.: Properties of Low-Aspect-Ratio Pointed Wings at Speeds Below and Above the Speed of Sound. NACA Rep. 835, 1946.
2. Ward, G. N.: Supersonic Flow Past Slender Pointed Bodies. Quart. Jour. of Mech. and Appl. Math., vol. II, pt. I, March 1949, pp. 75–97.
3. Ribner, Herbert S.: The Stability Derivatives of Low-Aspect-Ratio Triangular Wings at Subsonic and Supersonic Speeds. NACA TN 1423, 1947.
4. Spreiter, John R.: Aerodynamic Properties of Slender Wing-Body Combinations at Subsonic, Transonic, and Supersonic Speeds. NACA TN 1662, 1948.
5. Heaslet, Max. A., Lomax, Harvard, and Spreiter, John R.: Linearized Compressible-Flow Theory for Sonic Flight Speeds. NACA Rep. 956, 1950. (Formerly NACA TN 1824)
6. Lomax, Harvard, and Heaslet, Max. A.: Linearized Lifting-Surface Theory for Swept-Back Wings With Slender Plan Forms. NACA TN 1992, 1949.
7. Lamb, Sir Horace: Hydrodynamics. Dover Publications, New York, 6th ed., 1945, p. 60.
8. Lomax, Harvard, Heaslet, Max. A., and Fuller, Franklyn B.: Integrals and Integral Equations in Linearized Wing Theory. NACA Rep. 1054, 1951.
9. Prandtl, Ludwig: Recent Work on Airfoil Theory. Proceedings of Vth International Congress for Applied Mechanics, Cambridge, Mass., Sept. 1938. (Available as NACA TM 962, 1940)
10. Stewart, H. J.: The Lift of a Delta Wing at Supersonic Speeds. Quart. Appl. Math., vol. IV, no. 3, Oct. 1946, pp. 246–254.
11. Brown, Clinton E.: Theoretical Lift and Drag of Thin Triangular Wings at Supersonic Speeds. NACA Rep. 839, 1946.
12. Gurevich, M. I.: Lift Force of an Arrow-Shaped Wing. NACA TM 1245, 1949.
13. Falkner, V. M.: Calculated Loadings Due to Incidence of a Number of Straight and Swept-Back Wings. R. & M. No. 2596, British ARC, 1948.
14. Weissinger, J.: The Lift Distribution of Swept-Back Wings. NACA TM 1120, 1947.
15. DeYoung, John, and Harper, Charles W.: Theoretical Symmetric Span Loading at Subsonic Speeds for Wings Having Arbitrary Plan Form. NACA Rep. 921, 1948.
16. Berndt, Sune B., and Orlik-Rückemann, Kazimierz: Comparison Between Theoretical and Experimental Lift Distributions of Plane Delta Wings at Low Speeds and Zero Yaw. Swedish KTH TN 10, 1948.
17. Flax, A. H., and Lawrence, H. R.: The Aerodynamics of Low-Aspect-Ratio Wings and Wing-Body Combinations. Cornell Aero. Lab. Rep. No. CAL–37, Sept. 1951.
18. Lawrence, H. R.: The Lift Distribution on Low-Aspect-Ratio Wings at Subsonic Speeds. Cornell Aero. Lab. Rep. No. AF–673–A–1, Aug. 1950.
19. Berndt, Sune B.: Three Component Measurement and Flow Investigation of Plane Delta Wings at Low Speeds and Zero Yaw. Swedish KTH TN 4, 1948.
20. Lange and Wacke: Test Report on Three- and Six-Component Measurements on a Series of Tapered Wings of Small Aspect Ratio. (Partial report: Triangular Wing) NACA TM 1176, 1948.
21. Tosti, Louis P.: Low-Speed Static Stability and Damping-In-Roll Characteristics of Some Swept and Unswept Low-Aspect-Ratio Wings. NACA TN 1468, 1947.
22. Wick, Bradford H.: Chordwise and Spanwise Loadings Measured at Low Speed on a Triangular Wing Having an Aspect Ratio of 2 and an NACA 0012 Airfoil Section. NACA TN 1650, 1948.
23. Jones, Robert T.: Correction of the Lifting-Line Theory for the Effect of the Chord. NACA TN 817, 1941.

TABLE I.—VALUES OF CONSTANTS FOR EQUATION (35)

Const. \ $(\beta m)^2$	0	0.1	0.2
a_0	1.0000	1.0040	1.0513
a_1	0	.3151	.0168
a_2	0	−.6422	−.4481
γ	0	.010	.022

TABLE II.—VALUES CALCULATED FOR RIGHT SIDE OF EQUATION (33) USING EQUATION (35) AND TABLE I FOR $f_1(x_0)$

[Exact solution would, in each case, yield 1.000]

x_0	$(\beta m)^2=0.1$	$(\beta m)^2=0.2$
0.1	0.985	0.991
.2	1.000	1.000
.3	1.011	1.005
.4	1.022	1.004
.5	1.022	1.005
.6	1.016	1.007
.7	1.010	.999
.8	1.000	1.000
.9	.993	.997
.95	1.000	1.000

TABLE III.—RANGES OF PERTINENT PARAMETERS IN EXPERIMENTS

Reference number	Section shape	Thickness ratio (percent)	Reynolds number	Aspect ratios
13	(1)	10	(1)	4
19	Swedish FFA 104-5106	10	3×10^6	1,5/3,5/2
20	NACA 0012	12	1.7 to 3×10^6	1,4/3,2.3
21	(1)	(2 to 4)[1]	.4 to 9×10^6	(1,2,3)[1]
22	NACA 0012	12	2.4×10^6	2

[1] See text for explanation or qualification.

TABLE IV.—EXPERIMENTAL DATA ON LOW-ASPECT-RATIO TRIANGULAR WINGS TAKEN FROM REPORTS BY BERNDT (REFERENCE 19) AND LANGE AND WACKE (REFERENCE 20) (SEE TABLE III)

(a) Reference 19 (C_m referred to $\frac{1}{3}c_0$ and taken about point $\frac{1}{3}c_0$ back from apex)

$A=5/2$			$A=5/3$			$A=1$		
α	C_L	C_m	α	C_L	C_m	α	C_L	C_m
−3.7	−0.168	0.029	−4.8	−0.165	0.036	−4.2	−0.097	0.023
−2.7	−.122	.022	−3.8	−.130	.029	−3.2	−.072	.018
−1.7	−.075	.014	−2.8	−.096	.022	−2.2	−.049	.012
−.6	−.027	.006	−1.7	−.060	.015	−1.2	−.028	.007
.4	.020	−.002	−.7	−.023	.008	−.2	−.005	.002
1.5	.069	−.009	.3	.008	.002	.8	.018	−.003
2.5	.115	−.017	1.3	.043	−.005	1.8	.042	−.009
3.5	.160	−.024	2.3	.078	−.012	2.8	.064	−.014
4.6	.205	−.031	3.4	.114	−.019	3.8	.088	−.020
			4.4	.149	−.026	4.8	.110	−.025

(b) Reference 20 (C_m referred to $\frac{1}{3}c_0$ and taken about point $\frac{1}{3}c_0$ back from apex)

$A=1$			$A=4/3$		
α	C_L	C_m	α	C_L	C_m
−5.84	−0.1258	−0.0047	−5.81	−0.152	−0.0101
0	−.0002	−.0060 (sic)	0	.002	0
5.84	.1255	.0067	5.80	.156	.0089
$A=2$			$A=3$		
α	C_L	C_m	α	C_L	C_m
−5.71	−0.2375	−0.0177	−5.65	−0.2830	−0.0285
0	−.0180	−.0007	.02	−.0152	.0002
5.76	.1961	.0180	5.69	.2561	.0311